Optimization of Dividing Wall Distillation Columns

by

Colton Andrews

Submitted to

Dr. Robert B. Eldridge

And

Bailee J. Roach

McKetta Department of Chemical Engineering

Cockrell School of Engineering

The University of Texas at Austin

Spring 2017

Abstract

The dividing wall distillation column (DWC) is an energy efficient configuration, capable of a high purity tertiary separation within a single column.[1] DWC's are an alternative to the standard two distillation column configuration. A DWC includes additional degrees of freedom, making modeling and optimization more complex than standard distillation columns.[1] This study compiles results from previous DWC pilot columns into a process simulation to validate the method. Three pilot DWC columns were studied - the results of the three DWC column configurations (one four-product DWC and two three-product DWCs) were reconstructed using Aspen Plus™ and the product streams from the resulting simulations were compared to those provided in the authors' papers.[10-12] Each model is optimized using HEEDS®, a multidisciplinary optimization software that tests hundreds of design cases and analyze their results. From a base case simulation, the optimization software varied the DWC design parameters (number of stages, feed location, reboiler duty, etc.) across a specified range. Using the SHERPA optimization method, the objective function of HEEDS® was set to minimize/maximize the key process parameters used to design a DWC. From the simulations, the "best" design is determined, heat transfer is implemented, and a scale-up for each optimized design is conducted. HEEDS® in combination with Aspen Plus™ forms a powerful and efficient tool for the optimization of DWC simulations and designs and the reduction in time and simple user interface allows for many opportunities to test the various complicated design characteristics of the DWC.

Acknowledgements

I would like to acknowledge both my principal investigator, Dr. Robert B. Eldridge, and my graduate student, Bailee J. Roach, for the time, advice, and opportunity they have given me. I would also like to acknowledge the professors and faculty of the McKetta Department of Chemical Engineering within the Cockrell School of Engineering at The University of Texas at Austin for their work towards helping me complete my degree.

Table of Contents

List of Tables v

List of Figures vi

Introduction 1

Aspen Model 5

Literature Pilot Dividing Wall Distillation Columns Overview 9

D. Dwivedi's Four-Product Dividing Wall Distillation Column 9

M. I. A. Mutalib's Three-Product Dividing Wall Distillation Column 13

Fieg et al.'s Three-Product Dividing Wall Distillation Column 15

HEEDS Optimization Software 18

Linking Aspen to HEEDS 18

Methods of Optimization 21

Optimization Criteria 22

Heat Transfer & Scale-Up 23

Results and Discussion 26

Base Case Simulations 26

Dwivedi Base Case Simulation 26

Mutalib Base Case Simulation 27

Fieg Base Case Simulation 28

Optimized Column Results 29

Dwivedi's Column Results 29

Mutalib's Column Results 33

Fieg's Column Results 37

Heat Transfer & Scale-Up 40

Heat Transfer Implementation and Scale-Up of Dwivedi's Optimized Column 40

Heat Transfer Implementation and Scale-Up of Mutalib's Optimized Column 47

Heat Transfer Implementation and Scale-Up of Fieg's Optimized Column 51

Sources of Error 54

Conclusion 56

Appendix A – Symbols List 58

References 59

List of Tables

Table 1. Descriptions of Literature Pilot Dividing Wall Distillation Columns 9

Table 2. K-Values and relative volatilities for components in Dwivedi's column feed 12

Table 3. K-Values and relative volatilities of components in Mutalib's column feed 15

Table 4. K-values and relative volatilities of components in Fieg's column feed.17

Table 5. Optimized Dwivedi Column Design Variable Differences between Short-Range and Long-Range Methods.....22

Table 6. Base Case Simulation Results for Dwivedi's Column 27

Table 7. Base Case Simulation Results for Mutalib's Column 27

Table 8. Base Case Simulation Results for Fieg's Column.....28

Table 9. Effects of optimization on design variables for Dwivedi's Column 30

Table 10. Effects of optimization on design variables for Mutalib's Column.....34

Table 11. Effects of optimization on design variables for Fieg's column 37

Table 12. Simulation results of heat transfer implementation and scale-up for Dwivedi's optimized columns 41

Table 13. Liquid loading and vapor velocity for Dwivedi's optimized columns...47

Table 14. Simulation results of heat transfer implementation and scale-up for Mutalib's optimized column 48

Table 15. Liquid loading and vapor velocity for Mutalib's optimized columns....49

Table 16. Simulation results of heat transfer implementation and scale-up for Fieg's optimized column.....51

Table 17. Liquid loading and vapor velocity for Fieg's optimized columns.....52

List of Figures

Figure 1. Column configurations for ternary separation: (a) Direct Sequence, (b) Indirect Sequence, (c) Petyluk Configuration, (d) Dividing Wall Distillation Column.....2

Figure 2. Aspen process flowsheet for a three-product dividing wall distillation column.....5

Figure 3. Aspen process flowsheet for a four-product dividing wall distillation column.....7

Figure 4. D. Dwivedi's Pilot Scale Dividing Wall Distillation Column.....11

Figure 5. M. I. A. Mutalib's Pilot Scale Dividing Wall Distillation Column 14

Figure 6. Fieg et al.'s Pilot Scale Dividing Wall Distillation Column.....16

Figure 7. Scale-up methodology flowsheet 25

Figure 8. Liquid phase composition profile of the prefractionator for Dwivedi's optimized case.....31

Figure 9. Liquid phase composition profile for the rectifying, stripping, and main fractionator sections of Dwivedi's optimized column.....32

Figure 10. Liquid phase composition profile of the prefractionator for Mutalib's optimized column.....35

Figure 11. Liquid phase composition profile for the rectifying, stripping, and main fractionator sections of Mutalib's optimized column.....36

Figure 12. Temperature profile for Mutalib's optimized column 36

Figure 13. Liquid phase composition profile for the prefractionator of Fieg's optimized column.....38

Figure 14. Liquid phase composition profile of the rectifying, stripping, and main fractionator sections for Fieg's optimized column 38
Figure 15. Temperature profile for Fieg's optimized column 39
Figure 16. Temperature profile for Dwivedi's optimized column 42
Figure 17. Stage temperature difference between the base case simulation and the heat loss to the atmosphere simulation for Dwivedi's optimized 0.229 feet diameter column.....43
Figure 18. Stage temperature difference between the base case simulation and the heat loss to the atmosphere plus heat transfer across the wall simulation for Dwivedi's optimized 0.229 feet diameter column.....44
Figure 19. Stage temperature difference between the base case simulation and the heat loss to the atmosphere simulation for Dwivedi's optimized 10 feet diameter column.....45
Figure 20. Stage Temperature difference between the base case simulation and the heat loss to the atmosphere plus heat transfer across the wall simulation for Dwivedi's optimized 10 feet diameter column.....46
Figure 21. Standard column operation zones for packed distillation columns, as defined by KLM Technology Group[17].....49

Introduction

The first instance of a dividing wall distillation column (DWC) was published in 1949.[1] A DWC is a distillation column with a vertical wall inserted into the shell of the column and a side stream implemented on the side opposite of the feed. Standard distillation columns can separate a binary mixture into two high-purity product streams. Typically, ternary mixtures are separated using either the direct or indirect sequence of two distillation columns in series, as shown in Figure 1a and Figure 1b, respectively. However, the implementation of a vertical wall allows for the separation of a ternary mixture into three high-purity product streams within the shell of a single column, as shown in Figure 1d. The DWC is derived from the Petyluk configuration, where two columns are thermodynamically coupled, as shown in Figure 1c. The acronyms LK, MK, and HK in Figure 1 stand for light boiling key, middle boiling key, and heavy boiling key, respectively.

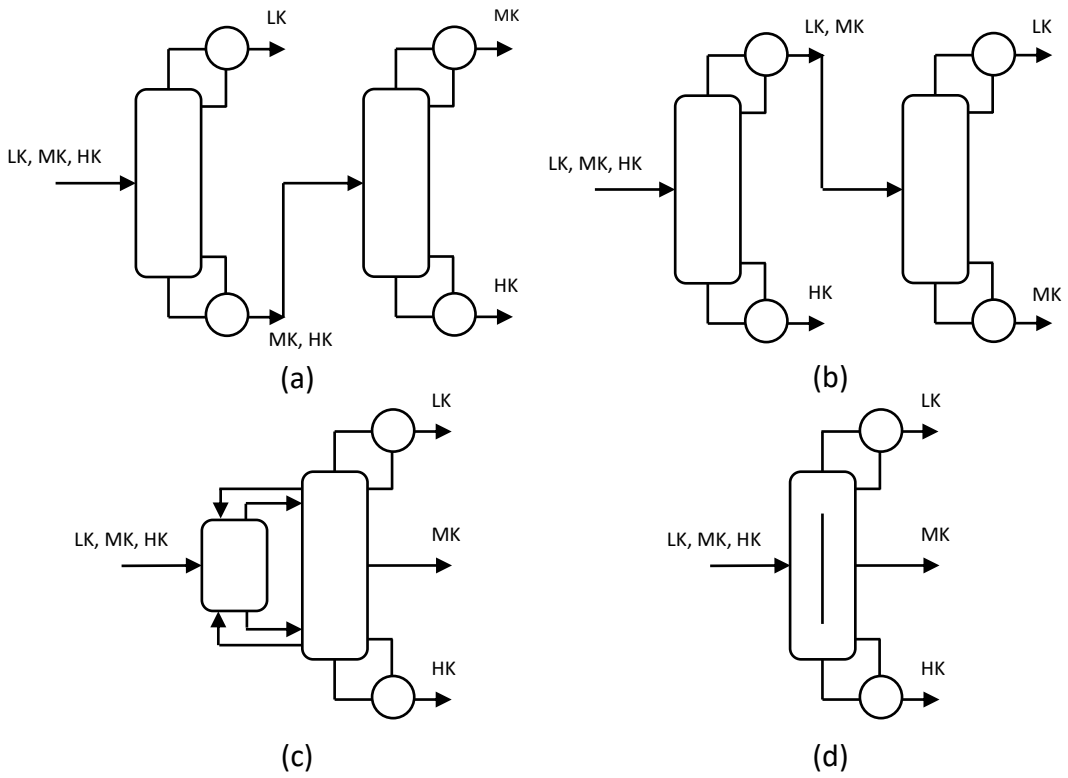

Figure 1. Column configurations for ternary separation: (a) Direct Sequence, (b) Indirect Sequence, (c) Petyluk Configuration, (d) Dividing Wall Distillation Column

Since the advent of DWCs, several authors have shown the energy saving and capital saving capabilities of DWC implementation in the place of traditional two-column configurations as upwards of 30-50%.[2-6] However, the introduction of a dividing wall and side stream within a single column shell introduces various new design parameters that increase the complexity of the design of DWCs. Several authors have attempted to address this problem with unique shortcut methods designed to obtain rough solutions to DWCs for certain classes of separations whereas others have addressed the optimizations of the base designs. This paper introduces a new method of optimization that can be used to yield optimized designs in terms of product purities and economic savings.

Several studies have presented different methods of optimization to find the optimal solution for DWC designs. Baldea et al. utilized networks of pseudo-transient differential-algebraic subunit models to simulate the various column sections and their interconnections.[7] Instead of iterating through each individual subunit, the material, equilibrium, summation, and heat (MESH) equations were solved simultaneously. The solution converged quickly and optimal design of all the subunits can be determined, but the rigorous mathematics employed can make modifications to the base DWC design cumbersome. Gomez-Castro et al. paired a multi-objective genetic algorithm, with restrictions based on the NSGA-Iland handling constraints, written in Matlab™, with the process simulator Aspen Plus™.[8] The genetic algorithm attempts to find the pareto front, or the set of optimal solutions from the minimum number of stages (infinite reflux ratio) to the minimum reflux ratio (infinite number of stages). The algorithm can be used to find a desirable solution that falls within this range and serves the chemical engineers desired design specifications. Kuo-Ksong Yu et al. takes it a step further with a systematic optimization method based on the genetic algorithm in conjunction with the radial basis function neural network.[9] Using the results of steady-state rigorous simulations as samples, an artificial neural network was trained to determine the relationship between the total annual cost and the design parameters of a DWC. Then, an objective function was evaluated with the neural network trained in the genetic algorithm. These studies showcase a trend of in-depth and complex mathematical modeling of DWCs. The goal of this paper is to determine the feasibility of HEEDS® as an optimization tool for DWC design and reduce the complexity of the approach to DWC optimization.

In this work, we assess the ability of HEEDS® in conjunction with Aspen Plus™ to optimize DWCs. This method is applied to three pilot columns found in literature, each with differing designs and feeds. Two of the columns are three-product DWCs with a single dividing

wall and one is a four-product DWC with a single dividing wall. For each column, a base case simulation that excludes heat loss is generated from the pilot column data to serve as the base case which HEEDS used to optimize. Once the optimized design is found, heat loss, both with and without heat transfer across the dividing wall, is incorporated into the design and the optimized columns are scaled up to 2 feet and 10 feet diameter columns. Finally, the designs of the optimized columns are evaluated and the conclusions are presented.

Aspen Model

Three DWCs were modeled in this study: two three-product DWCs and one four-product DWC. The process modeler used to simulate the steady-state operation of the three tested DWCs was Aspen Plus V8.8. The non-random two-liquid model was employed as the vapor-liquid equilibrium model for the separations. Aspen Plus does not have a rigorous process model specifically for DWCs. Thus, in order to model the DWCs studied, a combination of the available column types contained in Aspen Plus were used. A diagram of the process simulator user interface used for the three-product DWCs is shown in Figure 2.

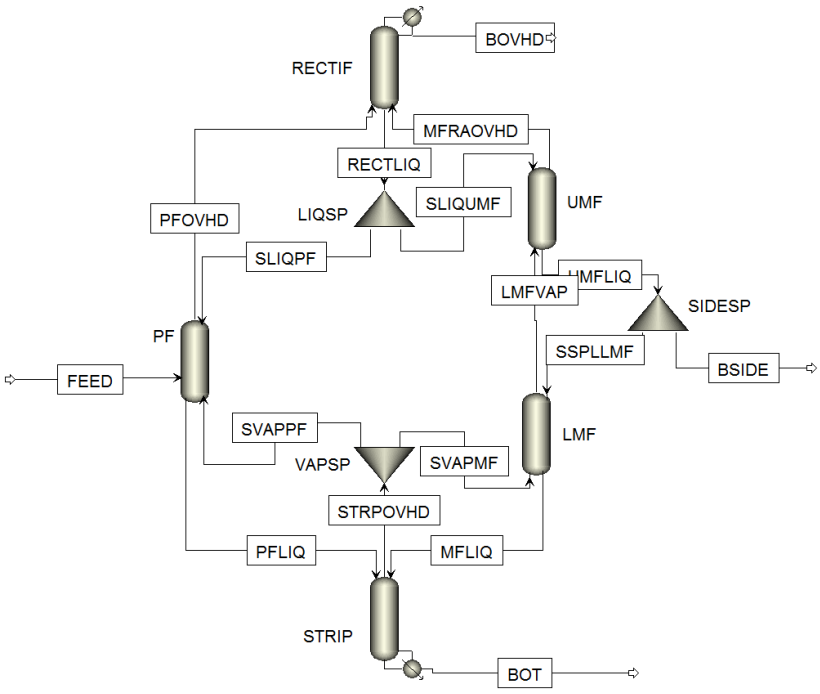

Figure 2. Aspen process flowsheet for a three-product dividing wall distillation column

The standard, rigorous distillation column model provided by Aspen Plus is the RadFrac block. In order to obtain a high accuracy simulation of the mass transfer and hydrodynamic phenomena, the DWC model consists of 5 separate RadFrac columns: one for the prefractionator,

one for the rectifying section (equilibrium stages above the wall plus the condenser), one for the stripping section (equilibrium stages below the dividing wall plus the reboiler), and two for the main fractionator. Vapor and liquid streams from each independent column section are attached to the respective adjacent column sections. To simulate the vapor and liquid splits as well as the side draw, FSplit separator blocks are used. For example, the vapor stream from the stripping section is split by the dividing wall into the prefractionator and main fractionator. Thus, the VAPSP block in Figure 2 splits the STRPOVHD vapor stream into SVAPPF and SVAPMF based on the vapor split value defined, creating the vapor streams that will feed the bottom of the prefractionator and main fractionator column sections, respectively. The inlet feed stream enters at a specified feed stage in the prefractionator and the product streams, distillate, side draw, and bottoms, are placed at the top of the rectifiying section, the outlet of the SIDESP FSplit block, and the bottom of the stripping section, respectively. Lastly, in all simulations, the reboiler type is kettle and the condenser is a total condenser.

For the four-product DWC modeled, six RadFrac blocks are used to model the various column sections, as shown in Figure 3.

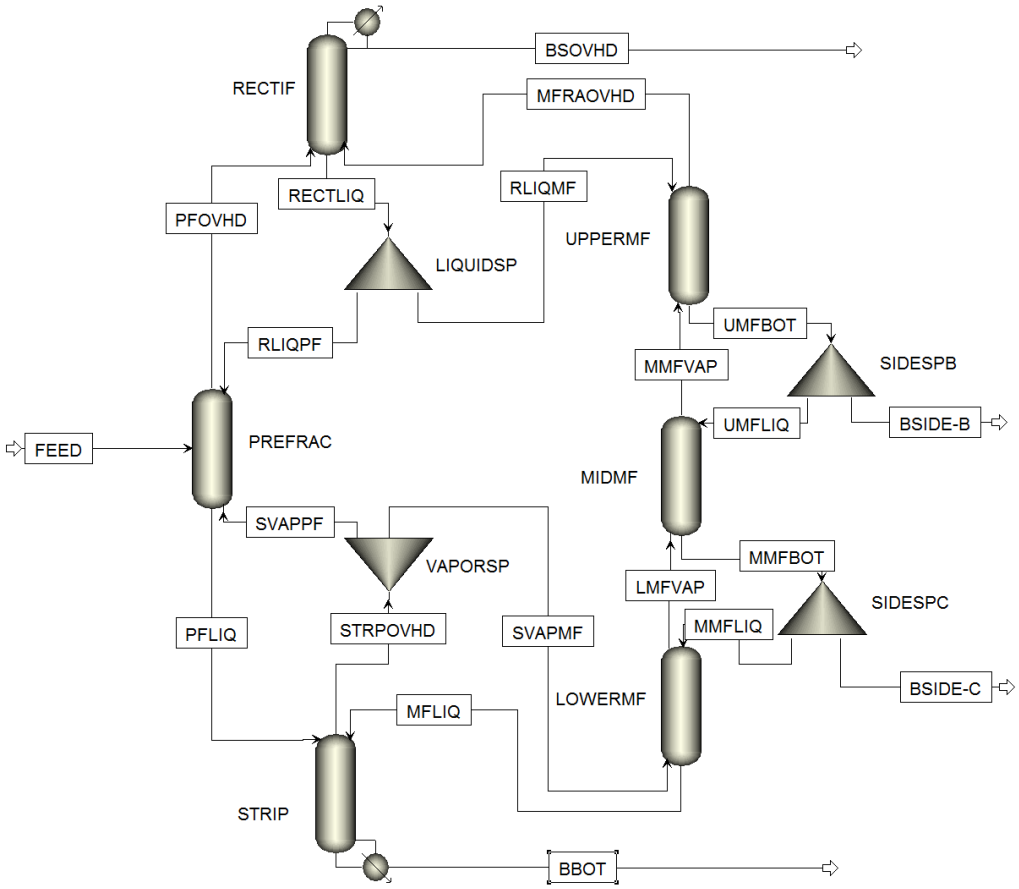

Figure 3. Aspen process flowsheet for a four-product dividing wall distillation column

An additional RadFrac block and FSplit block in the main fractionator section are required to model the four product lines leaving the DWC.

In the prefractionator and the main fractionator sections, the lack of a reboiler and condenser means that the degrees of freedom of these sections are lower than that of the stripping and rectifying sections, which each have an extra degree of freedom. In every column section, the number of stages, the feed and product stream locations, and the column section pressure are specified. In the rectifying section, the distillate flow rate is set to the feed flow rate multiplied by the light key fraction. In the stripping section, the reboiler duty is specified. For the liquid and vapor splits, the fraction of flow directed to the prefractionator is specified. Lastly, for the side

draw FSplit blocks, the flow rate of the side draw is set equivalent to the feed flow rate multiplied by the respective middle key.

For a DWC, different design variables are considered and can be modified to achieve a certain output from the column. For this study, it is important to note which variables were changed from simulation to simulation and which remained the same. Because the feed composition and flow rate remained the same for each simulation, the distillate and side draw flow rates are kept constant throughout all simulations. Also, the streams that connect two column sections fed/left a column section either above the first stage or on the last stage, respectively, simulating that the two column sections are connected as in a real DWC. Lastly, the condenser pressure, the feed pressure, and the pressure drop per stage were kept constant, using the pressures observed in the experimental pilot columns. Thus, the degrees of freedom that are varied are: feed temperature, prefractionator feed location, number of stages in a column section, vapor and liquid splits, and reboiler duty.

Literature Pilot Dividing Wall Distillation Columns Overview

Three columns were optimized using HEEDS in conjunction with Aspen Plus and, throughout the paper, are referred to by the name of the lead author of the publication. All of the columns studied are structured packing columns. Table 1 gives descriptions for each of the pilot columns.

Table 1. Descriptions of Literature Pilot Dividing Wall Distillation Columns

Main Author	Packing	Height (ft)	Diameter (ft)	System Studied	Wall Location
Dwivedi	6-mm Glass Raschig Rings	32.8	Rect./Strip. - 0.229 PF/MF - 0.16	Methanol/Ethanol/ Propanol/1-Butanol	Stages 5-16
Mutalib	GEMPAK 4A	36.0	1	Methanol/Isopropanol /1-Butanol	Stages 14-27
Fieg	Montz B1-500	39.4	0.22	1-Hexanol/1-Octanol/ 1-Decanol	Stages 6-15

D. Dwivedi's Four-Product Dividing Wall Distillation Column

The first column studied was a four-product, Kaibel column configuration constructed and operated by D. Dwivedi with results reported in his doctoral thesis titled "Control and operation of dividing-wall columns with vapor split manipulation."[10] A Kaibel column configuration is similar to a Petyluk configuration, except there are two side streams pulled from the main fractionator (MF) rather than one, resulting in the MF being split into three sections: the upper main fractionator (UMF), the middle main fractionator (MMF), and the lower main fractionator (LMF), as shown in Figure 4. Thus, there is a light key pulled from the distillate, two middle keys pulled from the side streams, and a heavy key pulled from the bottoms.

Typically, the liquid split and vapor split are set by the location of the dividing wall within the column shell. In the Dwivedi column, the separation of the PF and MF into separate shells

served as the physical separator that the dividing wall within a DWC typically causes. The flow area was split 50:50 to the PF and MF. However, Dwivedi implemented flow direction equipment that allowed manipulation of the liquid and vapor splits. Each section of the Dwivedi column had its own packing and, using collectors and distributors, directed the liquid and vapor flows through the packing.[10]

Dwivedi's column was not a true DWC as the column splits into two separate shells, one for the prefractionator (PF) and one for the main fractionator, above the stripping section. The two separate shells come back together at the top of the PF and MF to form the rectifying section of the DWC. Thus, there is no heat transfer between the PF and the MF in Dwivedi's experimental runs, a phenomenon that is characteristic to DWCs. A diagram of the pilot column with pertinent design variables is shown in Figure 4. The liquid and vapor splits denote what fraction of the flow is directed to the PF section of the column.

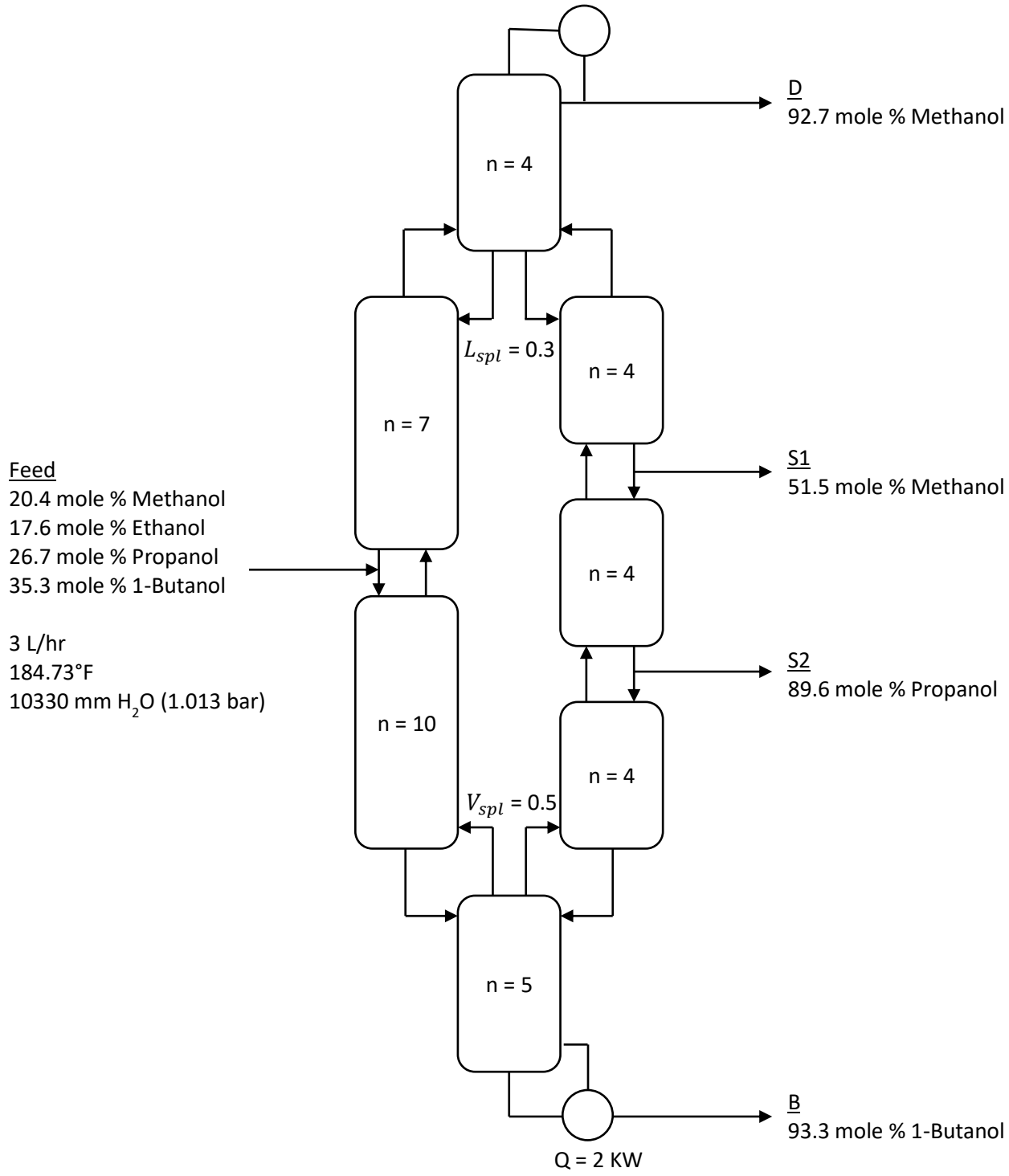

Figure 4. D. Dwivedi's Pilot Scale Dividing Wall Distillation Column

The K-values and relative volatilities for the four components at the feed temperature are shown in Table 2.

Table 2. K-Values and relative volatilities for components in Dwivedi's column feed

Component	K-Value	Rel. Volatility
Methanol	2.36	1.74
Ethanol	1.36	2.06
Propanol	0.66	2.06
1-Butanol	0.32	

The relative volatilities give an indication of the ease of separation between two components. In the Dwivedi alcohol feed, the hardest separation is between methanol and ethanol whereas the ethanol-propanol and propanol-1-butanol separations are relatively easier and similar in ease of separation.

M. I. A. Mutalib's Three-Product Dividing Wall Distillation Column

The pilot column studied in M. I. A. Mutalib's thesis, titled "Operation and Control of the Dividing Wall Column," was a three-product DWC separating a ternary mixture of alcohols: methanol, isopropanol, and 1-butanol.[11] All sections are contained within one shell with a vertical dividing wall separating the PF and MF, making the Mutalib column a true DWC. With one side draw, there is only an UMF and a LMF. The expected main components of the product streams are methanol in the distillate, isopropanol in the side draw, and 1-butanol in the bottoms.

The dividing wall in the Mutalib column was offset from the center such that the ratio of the MF flow area to the PF flow area was 1.29. Thus, the physical liquid and vapor splits, with respect to the fraction sent to the PF, are 0.437. A diagram of the Mutalib column with pertinent design variables is shown in Figure 5.

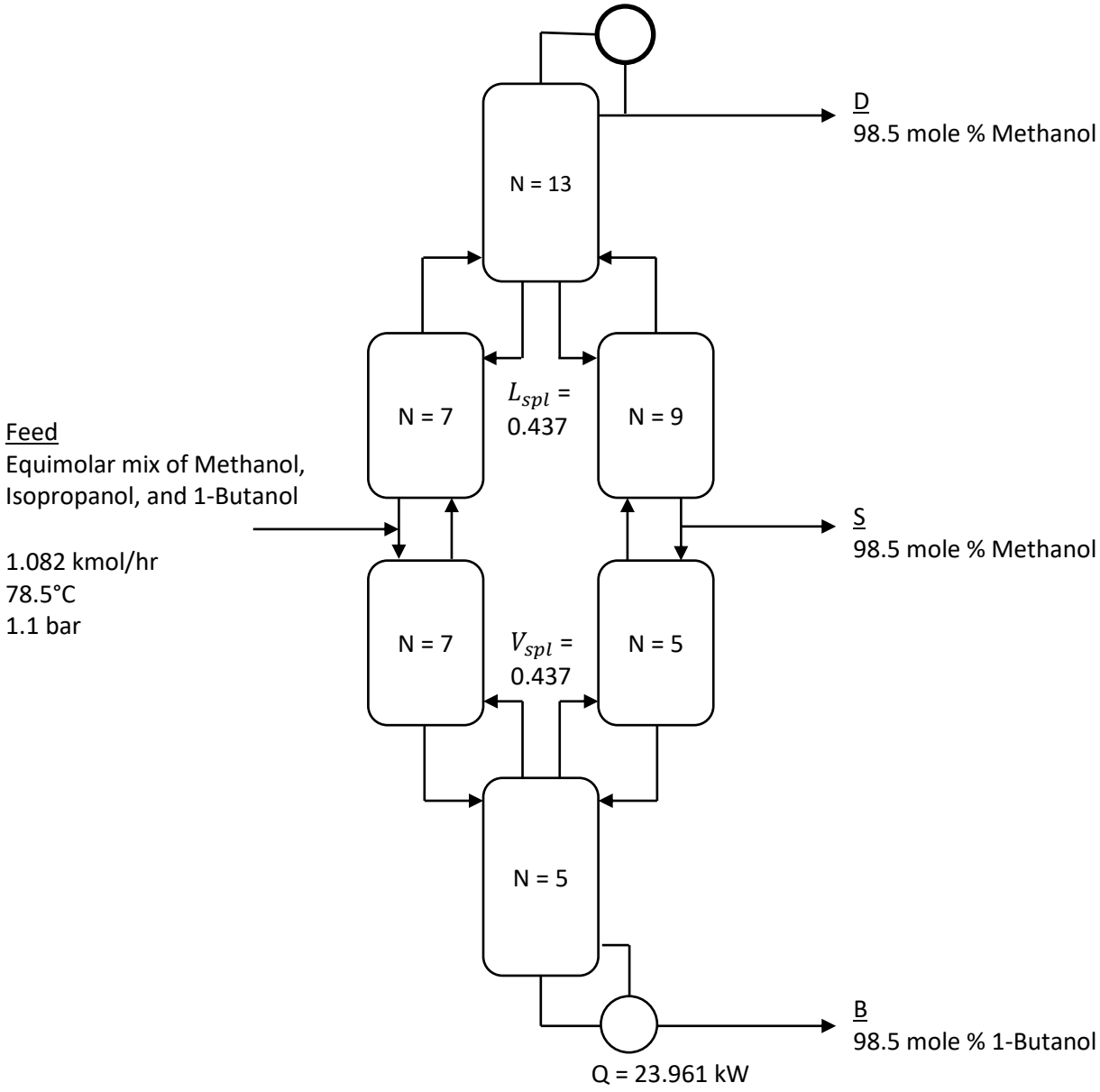

Figure 5. M. I. A. Mutalib's Pilot Scale Dividing Wall Distillation Column

Table 3 shows the relative volatilities for the Mutalib column feed components. From the relative volatilities, the methanol-isopropanol separation will require a larger energy input than the isopropanol-1-butanol separation.

Table 3. K-Values and relative volatilities of components in Mutalib's column feed

Component	K-Value	Rel. Volatility
Methanol	1.70	2.08
Isopropanol	0.82	
1-Butanol	0.18	4.54

FIEG ET AL.'S THREE-PRODUCT DIVIDING WALL DISTILLATION COLUMN

A three-product DWC pilot column presented and studied in "Experimental and Theoretical Studies of a Dividing-Wall Column Used for the Recovery of High-Purity Products" by Fieg et al. serves as the last DWC optimized in this paper.[12] The Fieg column separates a mixture of fatty alcohols, chosen because of their large production and importance for cosmetics, detergents, and colorants.[13] In order of decreasing volatility, they are 1-hexanol, 1-octanol, and 1-decanol. The dividing wall, like the Mutalib column, is welded in the middle of the column, separating the PF and the MF equally. A funnel acted upon by electromagnets is used to manipulate the liquid split whereas the vapor split is set by the dividing wall. A diagram showing the pertinent design parameters of the Fieg column is shown in Figure 6.

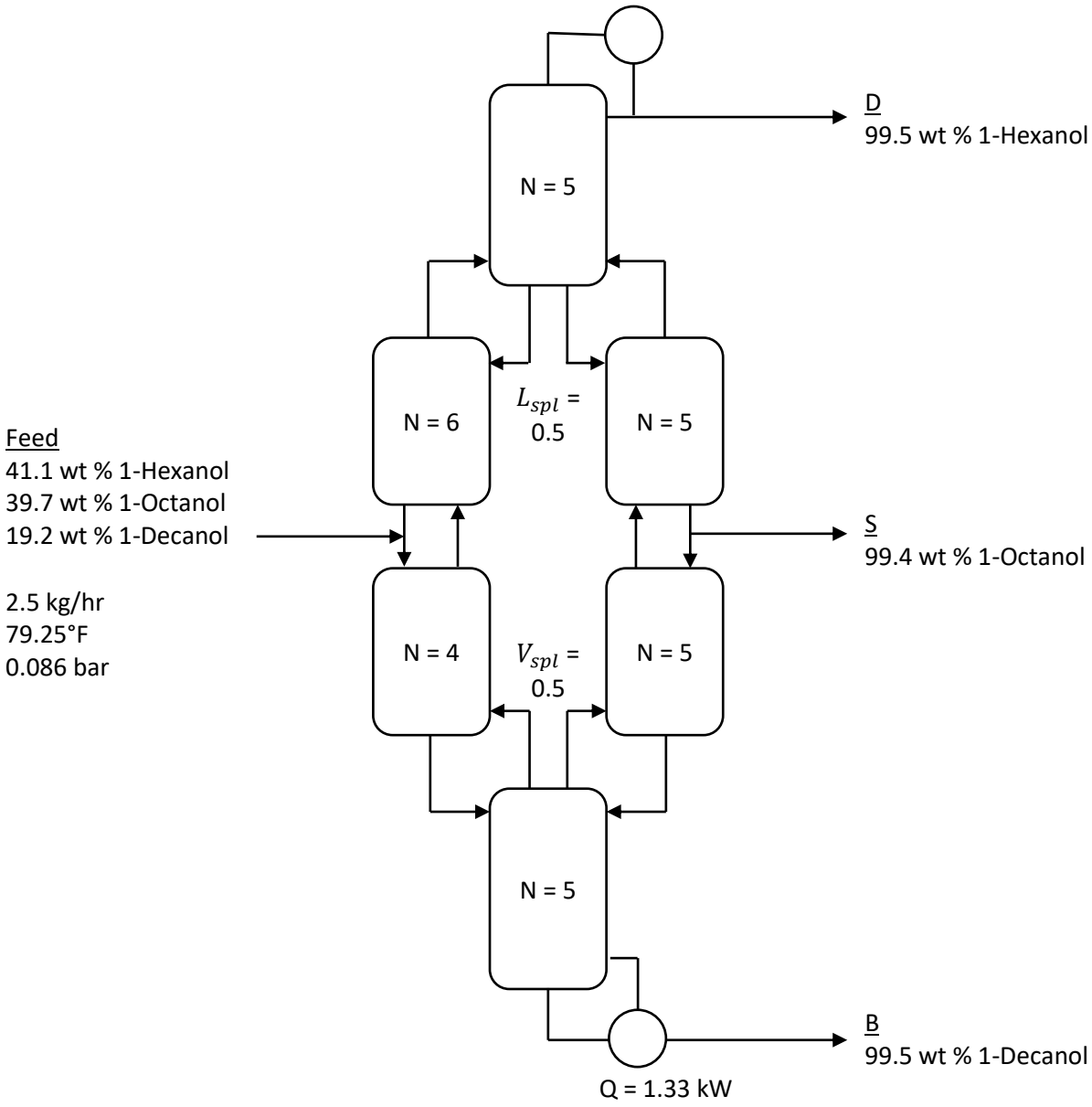

Figure 6. Fieg et al.'s Pilot Scale Dividing Wall Distillation Column

The K-values and relative volatilities for each component (or pair of components) are given in Table 4. Of the three feed systems, the Fieg feed system is, in theory, the easiest to separate.

Table 4. K-values and relative volatilities of components in Fieg's column feed

Component	K-value	Rel. Volatility
1-Hexanol	0.38	5.39
1-Octanol	0.07	
1-Decanol	0.01	5.04

HEEDS Optimization Software

HEEDS® is a multidisciplinary design exploration software produced by Red Cedar Technology that provides various optimization strategies as well as diverse connectivity to common commercial software, such as Excel.[13] This connectivity allows for HEEDS to generate input files of various types as well as read in outputs generated by other programs, which in turn can be analyzed and used to adjust new simulations executed by HEEDS. For example, during an optimization, a common goal is finding a minimum as an objective function. Depending on the user input, HEEDS can input desired values into the input file for a program, execute the program, and collect the output. The change in output, depending on how the input was changed, is analyzed and allows for HEEDS to adjust the input for the subsequent simulations to follow the trend required to achieve the objective function. In the case of the DWC, for example, if increasing the number of stages in the UMF increases the side product purity, HEEDS will choose higher values for the number of stages in the UMF for future simulations.

LINKING ASPEN TO HEEDS

Aspen Plus operates by setting up an environment that reads in an internal input file containing all of the pertinent design variables that the user has defined within the aspen (.apw) file.[14] Aspen Plus cannot directly link to HEEDS through the aspen file. However, an Aspen Plus simulation can be run through the command prompt in a method that essentially completes the task that the aspen file (.apw) does when a simulation is ran. Using a batch file that contains the required code for setting up the aspen environment, the command prompt can run simulations without the use of the standard Aspen Plus interface and .apw file if directed to an input file in a local directory containing the batch file. The result of this method is an output file that contains all of the

information pertaining to the simulation, the exact same that would be generated if the output file type of an aspen file were created.

The goal of using the command prompt to set up the Aspen Plus environment and execute a simulation is to have output text documents from which HEEDS can extract the data from the simulation as well as input text documents that HEEDS can generate and use to run new simulations. Thus, the methodology to running simulations is:

a. Generate a base case text input file that HEEDS can read and use as a baseline simulation.
b. Use the batch file to set up the Aspen Plus environment and run the simulation based on the information provided by the input file.
c. Generate a text output file.
d. From the output file, read in the results and evaluate the effect of the input variables on the output variables targeted by the objective functions

In the input file, the pertinent design variables to be altered are "tagged" within HEEDS, allowing HEEDS to modify certain values in the base line input file in order to generate new simulations. HEEDS is able to generate new simulations solely based off of the input file rather than having a user manually enter/change these values in the Aspen Plus user interface. For the output file, coding blocks within HEEDS allow for the extraction of the product purities and any other variables, the values of which are then used to analyze the efficacy of the change in the input variables.

After "tagging," the user can input the range and resolution of a certain input variable. The range defines the range of values that HEEDS will cover in a series of simulations and the resolution is the number of increments that the range of values is given. For example, if a range with a lower bound of 3 and a higher bound of 10 and a resolution of 8 is chosen for the number

of stages in the UMF section, then in the series of simulations executed by HEEDS, each integer value between 3 and 8, inclusive, can be tested. The product of the resolutions of all the input variables (the number of designs) dictates the total possible simulations that HEEDS can execute during a run.

HEEDS allows the user to categorize and separate simulations based on their results. Objective functions are used to guide the changes in inputs based on the optimization method chosen and constraints serve as a quick categorization method for the simulations that do not meet the minimum requirements set by the user. In the column simulations studied in this paper, the objective functions for all optimizations were to reduce the reboiler duty, to minimize the difference between the product purities and 0.99 (mole % or wt %, depending on the simulation), and to minimize the total number of stages in the column. When assessing the results, the objective function concerning the product purities was prioritized because, as in industry, obtaining a viable product is the most important function of a process. Constraints placed on some of the optimizations include categorizing those simulations with product purities higher than 0.99 mole/wt % as feasible and categorizing simulations that maintain the reboiler duty lower than a certain value as feasible.

HEEDS has the option to choose the optimization method. In this work, the SHERPA, or Simultaneous Hybrid Exploration that is Robust, Progressive, and Adaptive, method was used.[16] The SHERPA method is unique in that it simultaneously uses multiple search methods in a single search to obtain the best results possible by taking advantage of the best attributes of one method while minimizing the disadvantages of a method by suppressing its participation in the search. In other words, SHERPA effectively removes the arduous task of selecting a search method based on

the problem statement/design space and is able to use the results of its generated simulations to guide the simultaneous search methods towards the optimal solution.

Methods of Optimization

When designating the ranges for the input variables of a series of simulations, two apparent approaches can be used: a short-range or a long-range method. The main differences between the two methods is the size of the range chosen for each input variable and the number of simulations conducted during a run. Each variable must be treated differently depending on the variable type. For example, stage numbers are discrete whereas the reboiler duty is continuous. For the short-range method, smaller ranges are chosen for each run and the number of simulations for the run is lower. After each run, the results are evaluated, a new baseline is chosen and the ranges for the variables that changed between the two baselines are adjusted with respect to the new baseline values. The short-range method allows for less time spent per run and more flexibility in terms of the direction of the optimization. The long-range method dictates that much larger ranges are chosen and the number of simulations per run are increased to accommodate for the increase in range. This method allows for HEEDS to search over a larger design space, but loses the guided direction that the short-range method offers.

Both methods were tested on each column to determine which method was better for finding the global optimum solution. For the Fieg column, both methods arrived at the same solution whereas for the Dwivedi and Mutalib columns, the long-range method was able to locate more optimal solutions. The following Table 5 shows the differences between the optimum solutions found by the short-range and the long-range methods for the Dwivedi column.

Table 5. Optimized Dwivedi Column Design Variable Differences between Short-Range and Long-Range Methods

Variable	Short Range	Long Range	Percent Diff. (%)
Distillate Methanol Purity (%)	99.9	99.9	0.0
Side Draw 1 Ethanol Purity (%)	99	99.1	0.1
Side Draw 2 Propanol Purity (%)	99.3	99.3	0.0
Bottoms 1-Butanol Purity (%)	99.9	99.9	0.0
Reboiler Duty (kW)	2.60	1.74	-33.1
Feed Temperature (F)	184	185	0.5
PF Number of Stages	26	19	-26.9
Feed Stage (Above Stage)	18	11	-38.9
Rectifying Number of Stages	16	16	0.0
UMF Number of Stages	15	15	0.0
MMF Number of Stages	14	16	14.3
LMF Number of Stages	15	10	-33.3
Stripping Number of Stages	14	14	0.0
Total Number of Stages	100	90	-10.0
Liquid Split	0.26	0.24	-7.7
Vapor Split	0.31	0.32	3.2

The long-range method was able to find the better optimal solutions, with a 10% decrease in the optimal total number of stages as well as a 33% decrease in the optimal reboiler duty. As the DWC is a multivariable system, the long-range method is better equipped to finding the global, rather than a local, minimum.

Optimization Criteria

In each optimization, the optimization criteria that guided HEEDS towards the best design were the same for each column. The goal of the optimization was to find a design that met the product purity requirement of 99 mol/wt% in each of the product streams while at the same time, reducing the capital costs and energy requirements of the column. The main variables affecting capital costs are the column diameter, column height, and number of stages in the column whereas

the energy requirements are related to the reboiler and condenser duties. However, the only variables that were directly influenced by HEEDS are the total number of stages and the reboiler duty. Thus, the capital cost is correlated to the total number of stages and the energy requirement is correlated to the reboiler duty. The objective function in HEEDS was set to minimize the values of both variables. The total number of stages is defined as shown in Equation 1.

$$N_{tot} = N_{Rect} + N_{PF} + N_{MF} + N_{Strip} \qquad \textit{Equation 1. Total Number of Stages}$$

For the product purities, minimizing the difference between the product stream purity and 0.99 was set as the objective function. Constraints were set that tagged only the simulations with all three (or four) product streams with 99 mol/wt% as feasible. Any simulations with at least one stream with a purity under 0.99 were tagged as functional, but infeasible designs. The best (optimized) case is chosen from the feasible designs as the simulation with the least total number of stages and the lowest reboiler duty.

HEAT TRANSFER & SCALE-UP

For each case, more designs (simulations), one including only heat loss to the atmosphere and one including both heat loss to the atmosphere and heat transfer across the dividing wall, were generated to observe the change in reboiler duty as well as other design variables. Each of these cases were also scaled-up to 2 feet and 10 feet diameter columns, representing industrial sized columns. The optimized case served as the base case for the heat transfer and scale-up simulations. To calculate the heat loss/transfer, the standard heat transfer equation, Equation 2, was used with the temperatures from the optimized simulation.

$$\dot{Q} = UA(T_{wall} - T_o) \qquad \textit{Equation 2. Heat transfer}$$

More assumptions made include the atmospheric temperature, T_o, is 70°F, the overall heat transfer coefficient to the atmosphere is $U_{atm} = 14\ W/m^2 \cdot K$, and the overall heat transfer

coefficient for the wall is $U_{wall} = 300\ W/m^2 \cdot K$. None of the authors provided overall heat transfer coefficient values for their columns, so these values were chosen as they are averages observed in the UT Austin DWC pilot column. There can be error in the heat transfer caused by using the base case temperature profile, which will be discussed with each individual case

The scale-up process is shown in Figure 7. Depending on the simulation, the heat loss to the atmosphere and the heat transfer across the wall are calculated based on the optimized case temperatures and the heat transfer area (calculated depending on the diameter set for the column). The reflux ratio for the distillate stream (R_R) and the liquid loading in the rectifying section (L_{Rect}) are calculated. These values are compared to the distillate reflux ratio and rectifying section liquid loading of the base case and, if the values do not match, the reboiler duty and feed flow rate (as well as the distillate and side stream(s) flow rates) are adjusted. Once the values match, the scale-up process is complete.

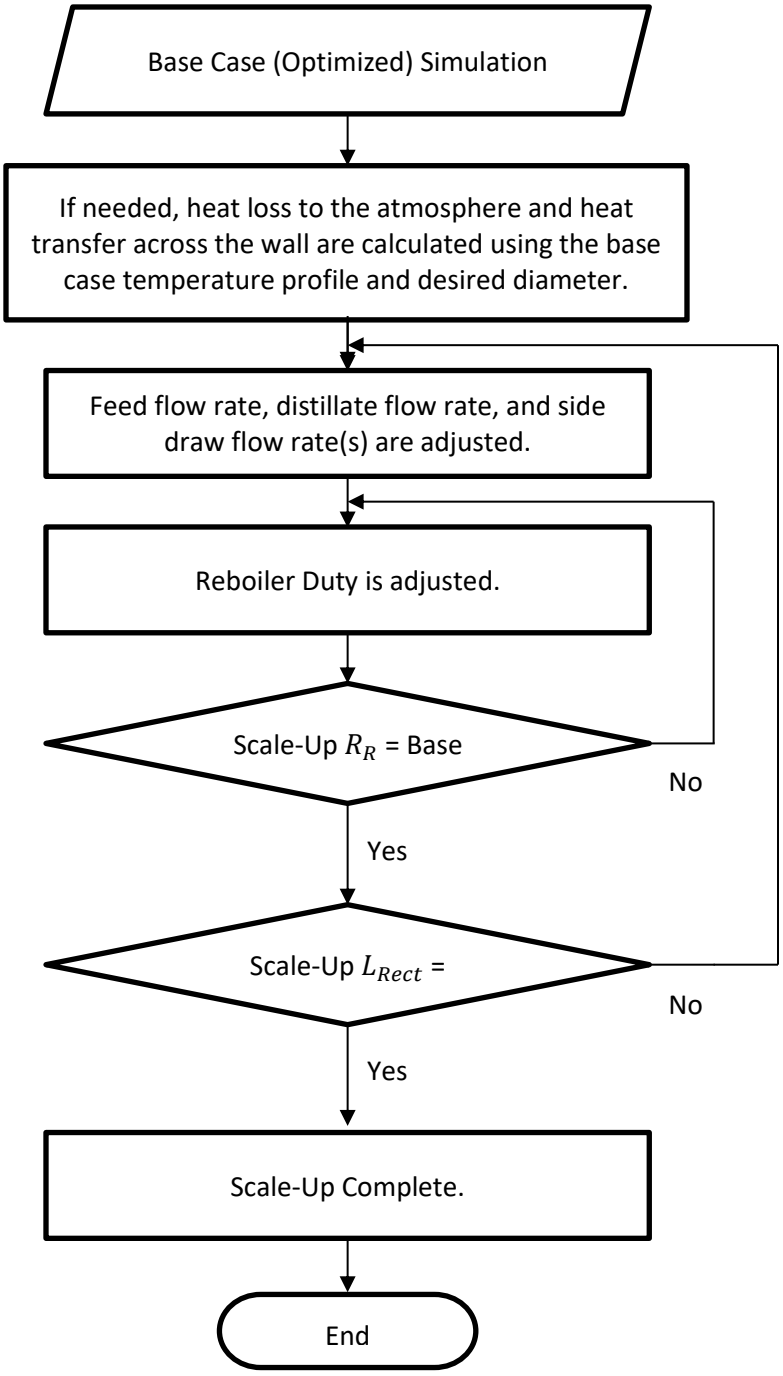

Figure 7. Scale-up methodology flowsheet

Results and Discussion

In this section, the base case and optimized columns are discussed. The operation of each optimized column is studied, followed by an implementation of heat transfer in each column, both with heat loss to the atmosphere and with heat transfer across the wall. Lastly, the columns are scaled-up and the hydraulics within each column is discussed.

Base Case Simulations

In order to optimize the studied columns, it is necessary to generate a base case aspen simulation that can model the pilot scale DWC. The values for the design variables given in the literature were used as starting points and, with a few minor adjustments, a base case simulation was generated in aspen. The results of each base case simulation, and how they compare with the simulation/experimental results in literature, will now be discussed.

Dwivedi Base Case Simulation

Experiment run 11, as is denoted in Dwivedi's thesis, was the case studied and optimized in this paper. The feed to the column was a mixture of the four lowest molecular weight, linear chain alcohols: methanol, ethanol, propanol, and 1-butanol. Listed in order of decreasing volatility, the expected main component in each of the product streams are methanol in the distillate, ethanol in side draw 1, propanol in side draw 2, and 1-butanol in the bottoms. As is evident by the purity of the streams, the design was unable to achieve four high-purity product streams. Dwivedi's column was simulated in Aspen Plus, to serve as the base case of optimization for HEEDS. The design parameters required a few minor adjustments to generate a successful run. The reboiler duty was changed to 2.5 KW and the liquid and vapor splits were adjusted to 0.25 and 0.35, respectively.

The resulting stream purities are shown in Table 6. It should be noted that heat transfer across the dividing wall and heat loss to the environment is not accounted for in the base simulation.

Table 6. Base Case Simulation Results for Dwivedi's Column

	Feed		D		S1		S2		B	
Comp.	Dwivedi	Sim	Dwivedi	Sim	Dwivedi	Sim	Dwivedi	Sim	Dwivedi	Sim
Methanol	20.4	20.4	92.7	88.4	17.3	17.8	0	0.7	0	0
Ethanol	17.6	17.6	7.3	11.2	51.5	59.5	5.4	18.4	0	0
Propanol	26.7	26.7	0	0.4	31.2	22.6	89.6	77.8	6.7	3.1
1-Butanol	35.3	35.3	0	0	0	0.1	4.9	3.1	93.3	96.9

Adjusting design parameters will result in changes in the purities of the stream, but the general trend of higher purities in the distillate and bottom streams is observed.

Mutalib Base Case Simulation

The Mutalib column was simulated using Aspen Plus to obtain a base case simulation from which HEEDS can optimize. With a minor reduction in the reboiler duty to 20.5 kW, the stream purities of both Mutalib' simulation and the simulation generated are shown in Table 7. It should be noted that neither heat transfer across the wall nor heat loss to the environment are accounted for in the simulation as well as in Mutalib's simulation.

Table 7. Base Case Simulation Results for Mutalib's Column

	Feed		D		S		B	
Comp.	Mutalib	Sim	Mutalib	Sim	Mutalib	Sim	Mutalib	Sim
Methanol	33.3	33.3	98.5	92.8	1.3	7.2	0	0
Isopropanol	33.3	33.3	1.5	7.2	98.5	92.0	1.5	0.8
1-Butanol	33.3	33.3	0	0	0.2	0.8	98.5	99.2

Our simulation showed the distillate and side draws having larger levels of impurities of the middle key and light key, respectively. The bottoms purity was the closest between the two simulations, being off by 0.7%.

Fieg Base Case Simulation

Out of the cases presented in Fieg et al.'s paper, case A was chosen as the case to optimize in this study. The feed and product stream main component compositions are 1-hexanol for the distillate, 1-octanol for the side draw, and 1-decanol for the bottoms. When simulated in Aspen Plus, the simulation product streams agreed well, as shown in Table 8.

Table 8. Base Case Simulation Results for Fieg's Column

	Feed		D		S		B	
Comp.	Fieg	Sim	Fieg	Sim	Fieg	Sim	Fieg	Sim
1-Hexanol	41.1	41.1	99.5	99.6	0.6	0.2	0	0
1-Octanol	39.7	39.7	0.5	0.4	99.4	99.5	0.5	0.7
1-Decanol	19.2	19.2	0	0	0	0.3	99.5	99.3

Optimized Column Results

Using the HEEDS + Aspen Plus optimization method, each base case simulation served as the starting point from which the column was optimized. The results of the method on the optimized columns will now be discussed.

Dwivedi's Column Results

The results of the optimized Dwivedi column are shown in Table 9, with the percent change in each design variable between the base case and the optimized case. In order to achieve higher purities in the four product streams, the column grew in every section, specifically the main fractionator, with increases in the number of stages upwards of 325%. The increase in equilibrium stages was required to separate the four components and achieve the 99 mole % minimum. An increase in the number of stages inherently means an increase in the capital cost of the column required to achieve the high purities. In terms of operating costs, the reboiler duty, feed temperature, reflux ratios and splits are pertinent. The reboiler duty was reduced, even with an increase in the equilibrium stages, showing more effective mass transfer was required to improve the separation rather than an increase in the required energy. The reflux ratio in the rectifying section as well as both side stream reflux ratios decreased. The liquid and vapor splits adjusted to the values that resulted in the lowest reboiler duty, though the percent change is nearly negligible besides the vapor split setting the location of the wall, which is only a minor incurred cost.

Table 9. Effects of optimization on design variables for Dwivedi's Column

Variable	Base Case	Optimized	Percent Change (%)
Distillate Methanol Purity (%)	88.4	99.9	13.0
Side Draw 1 Ethanol Purity (%)	59.5	99.1	66.6
Side Draw 2 Propanol Purity (%)	77.8	99.3	27.6
Bottoms 1-Butanol Purity (%)	96.9	99.9	3.1
Reboiler Duty (kW)	2.50	1.74	-30.4
Feed Temperature (F)	184.73	185	0.1
PF Number of Stages	17	19	11.8
Feed Stage (Above Stage)	8	11	37.5
Rectifying Number of Stages	4	16	300.0
UMF Number of Stages	4	15	275.0
MMF Number of Stages	4	16	300.0
LMF Number of Stages	4	10	150.0
Stripping Number of Stages	5	14	180.0
Total Number of Stages	38	90	136.8
Reflux Ratio	30.3	19.8	-34.7
Side 1 Reflux Ratio	23.4	15.8	-32.5
Side 2 Reflux Ratio	13.3	9.1	-31.6
Liquid Split	0.25	0.24	-4.0
Vapor Split	0.35	0.32	-8.6

An efficient four-product DWC would have separation of the two lighter components from the two heavier components within the prefractionator. Figure 8 shows the liquid compositions at each stage for the prefractionator.

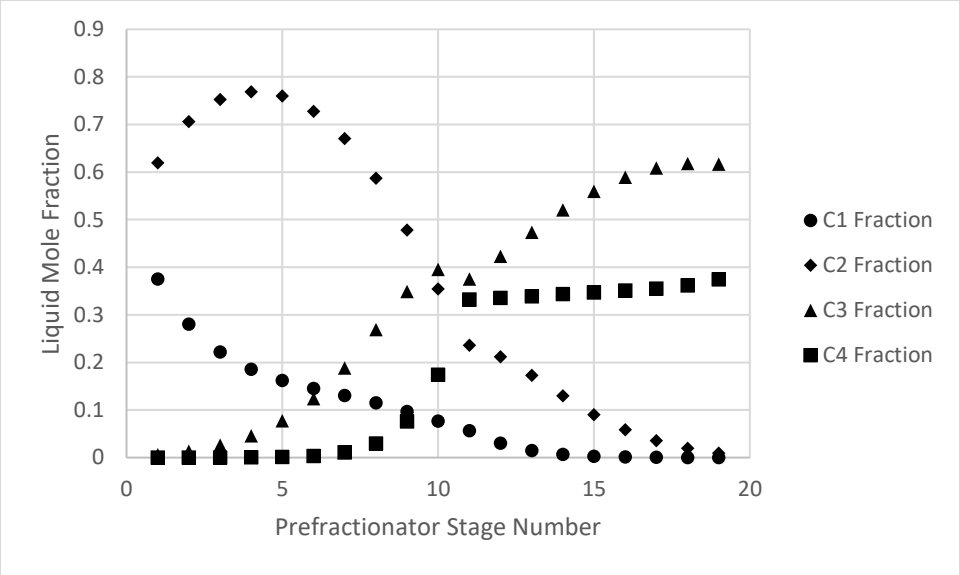

Figure 8. Liquid phase composition profile of the prefractionator for Dwivedi's optimized case

In the optimized case, the vapor leaving the prefractionator at the top is nearly all methanol and ethanol, with a slight 0.14 mole % propanol impurity. Similarly, the liquid leaving the prefractionator at the bottom is nearly all propanol and 1-butanol, with a small 0.06 mole % ethanol impurity.

Figure 9 shows the liquid compositions throughout the rectifying section, main fractionator sections, and the stripping section.

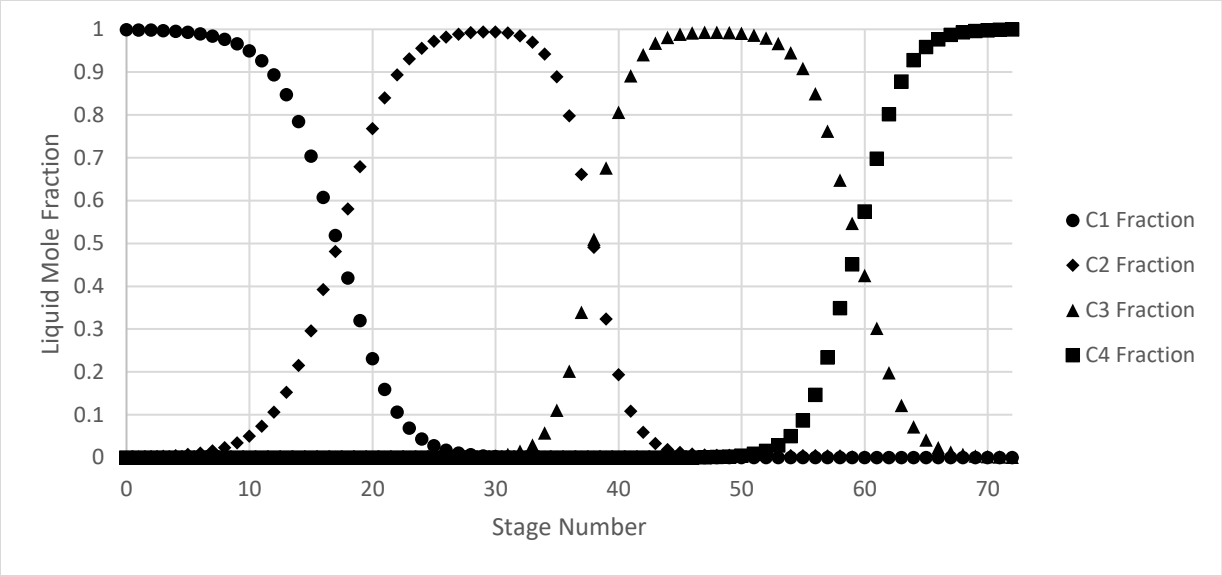

Figure 9. Liquid phase composition profile for the rectifying, stripping, and main fractionator sections of Dwivedi's optimized column

The side draw locations are placed between the stages at which the ethanol and propanol mole fractions are highest, respectively. The rectifying section separates the methanol from the ethanol, yielding the high purity distillate, and splits the returning ethanol between the prefractionator and the main fractionator. The upper main fractionator separates the ethanol from the methanol and returns methanol back to the rectifying section. Streams entering the middle main fractionator contain relatively high purity ethanol and propanol, which are mixed throughout this section. The middle main fractionator ensures that the ethanol is redirected back towards side draw 1 and propanol is redirected back towards side draw 2. From before, the liquid leaving the prefractionator (mainly propanol and 1-butanol) is sent to the stripping section where the 1-butanol is separated from the propanol. Propanol is directed either back into the prefractionator or into the lower main fractionator, where propanol is separated from 1-butanol and 1-butanol is sent back to the stripping section.

Referring back to table 2, the relative volatilities between each neighboring component gives an indication of the relative size of each section. The harder the separation, the more equilibrium stages required in the section separating the components. Thus, according to the relative volatilities, the rectifying section and UMF combined should have more stages than the stripping section and LMF combined, which is this case with 31 stages versus 24 stages.

Mutalib's Column Results

Table 10 shows the results of the optimized case for Mutalib's column compared to the base case. Similar to Dwivedi's column, the optimized Mutalib column showed an increase in theoretical tray count in nearly all of the column sections, though not as drastically with 53.8% being the largest change. The operating costs-related design variables all experienced decreases, a good indication of a well optimized column. The reboiler duty was reduced by nearly 25% whereas the reflux ratio and side reflux ratio reduced were by -31.1% and -16.7%, respectively.

Table 10. Effects of optimization on design variables for Mutalib's Column

Variable	Base Case	Optimized	Percent Change (%)
Distillate Methanol Purity (%)	92.8	99.2	6.9
Side Draw Isopropanol Purity (%)	92	99.1	7.7
Bottoms 1-Butanol Purity (%)	99.2	99.9	0.7
Reboiler Duty (kW)	20.5	15.4	-24.9
Feed Temperature (F)	78.5	78.5	0.0
PF Number of Stages	14	17	21.4
Feed Stage (Above Stage)	8	10	25.0
Rectifying Number of Stages	13	20	53.8
UMF Number of Stages	9	9	0.0
LMF Number of Stages	5	7	40.0
Stripping Number of Stages	5	6	20.0
Total Number of Stages	46	59	28.3
Reflux Ratio	4.5	3.1	-31.1
Side Reflux Ratio	1.2	1.0	-16.7
Liquid Split	0.437	0.75	71.6
Vapor Split	0.437	0.42	-3.9

Table 3 gives the K-values and relative volatilities of adjacent components at the feed temperature for the components being separated in the Mutalib column. From the relative volatilities, the methanol-isopropanol separation requires more energy/mass transfer than the isopropanol-1-butanol separation. Thus, the rectifying section plus UMF section (29 stages) is larger than the stripping section plus LMF section (13 stages). The prefractionator separates methanol from 1-butanol, with isopropanol being split to both the rectifying and stripping sections, as shown in Figure10.

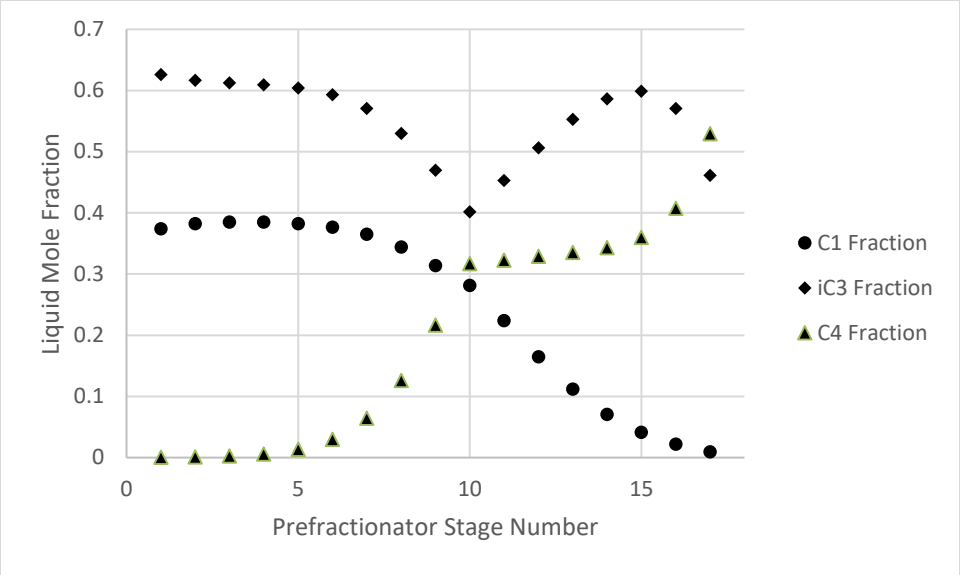

Figure 10. Liquid phase composition profile of the prefractionator for Mutalib's optimized column

The rectifying section, where methanol is separated from isopropanol, comprises a majority of the column. The stripping section separates 1-butanol from isopropanol and isopropanol is separated from methanol and 1-butanol in the UMF and LMF, respectively. The side draw location is set by the point in the column where the isopropanol fraction is highest.

It is worth noting the liquid and vapor splits and their difference. In the optimized case, slightly more than 40% of the vapor from the stripping section is directed to the prefractionator whereas 75% of the liquid coming from the rectifying section is sent to the prefractionator. In Dwivedi, the majority of both the vapor and liquid flow from the stripping and rectifying sections, respectively, are sent to the main fractionator even though these separation systems are relatively similar with low molecular weight alcohols.

The temperature profile, in Figure 12, shows large differences in the temperature changes between the top and bottom of the column, an indication of the relative ease of separation of the three components. The components of the more difficult methanol-isopropanol separation have

similar boiling temperatures, explaining the lack of change in the temperature, and composition as shown in Figure 11, in the rectifying section, whereas the easier isopropanol-1-butanol separation shows a spike in the temperature and large changes in compositions within a smaller range of stages.

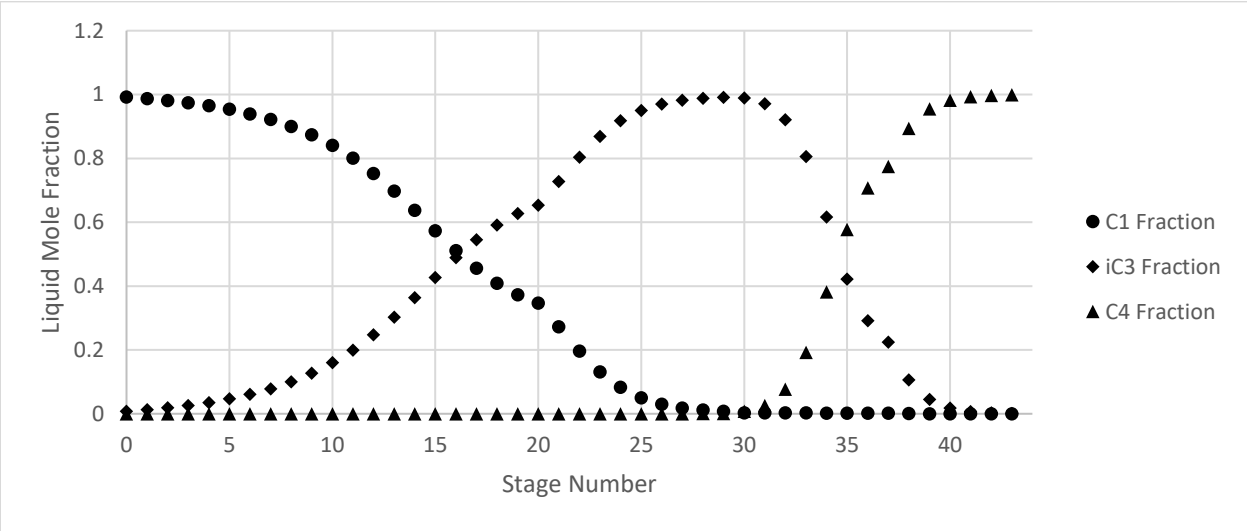

Figure 11. Liquid phase composition profile for the rectifying, stripping, and main fractionator sections of Mutalib's optimized column

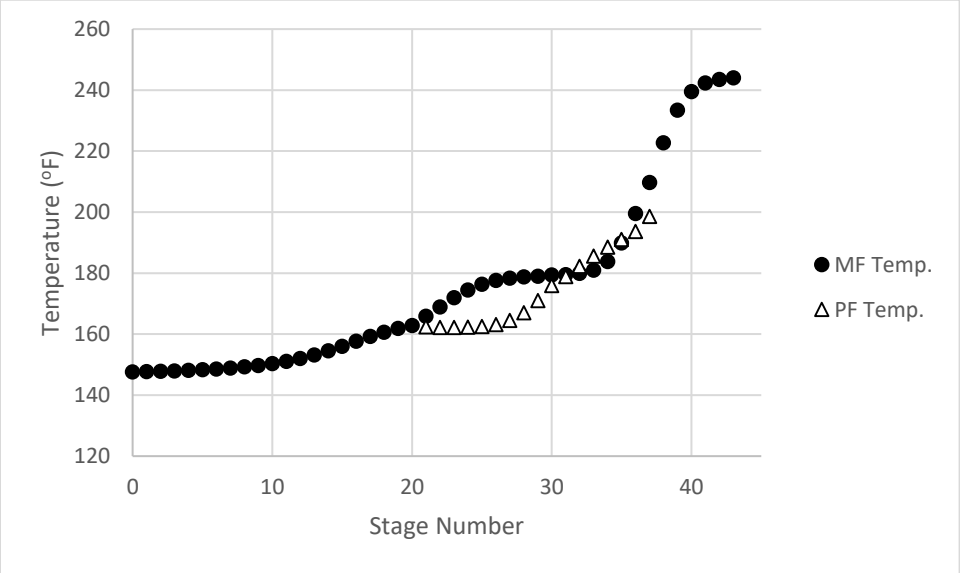

Figure 12. Temperature profile for Mutalib's optimized column

Fieg's Column Results

The last DWC optimized was the Fieg column, the results of which are shown in Table 11. The Fieg column was the only optimized column with a reduction in the total number of stages. The prefractionator was reduced to half the original size. The rectifying section and LMF changed slightly as well. In terms of the design variables related to energy cost, the reboiler duty decreased to nearly half of its original value, most likely the result of the increased feed temperature. The reflux ratio and side draw reflux dropped 51.1% and 36.7% as well. Lastly, the liquid split adjusted whereas the vapor split remained constant.

Table 11. Effects of optimization on design variables for Fieg's column

Variable	Base Case	Optimized	Percent Change (%)
Distillate 1-Hexanol Purity (%)	99.6	99.1	-0.5
Side Draw 1-Octanol Purity (%)	99.5	99.1	-0.4
Bottoms 1-Decanol Purity (%)	99.3	99.3	0.0
Reboiler Duty (kW)	1.33	0.73	-45.1
Feed Temperature (F)	79.25	168.53	112.7
PF Number of Stages	10	5	-50.0
Feed Stage (Above Stage)	6	2	-66.7
Rectifying Number of Stages	5	4	-20.0
UMF Number of Stages	5	5	0.0
LMF Number of Stages	5	6	20.0
Stripping Number of Stages	5	5	0.0
Total Number of Stages	30	25	-16.7
Reflux Ratio	4.7	2.3	-51.1
Side Reflux Ratio	3	1.9	-36.7
Liquid Split	0.5	0.27	-46.0
Vapor Split	0.5	0.5	0.0

With a ternary feed, the Fieg column is expected to operate very similarly to Mutalib's column. Figures 13 and 14 show the liquid compositions throughout the prefractionator and the rectifying section, main fractionator, and stripping section, respectively.

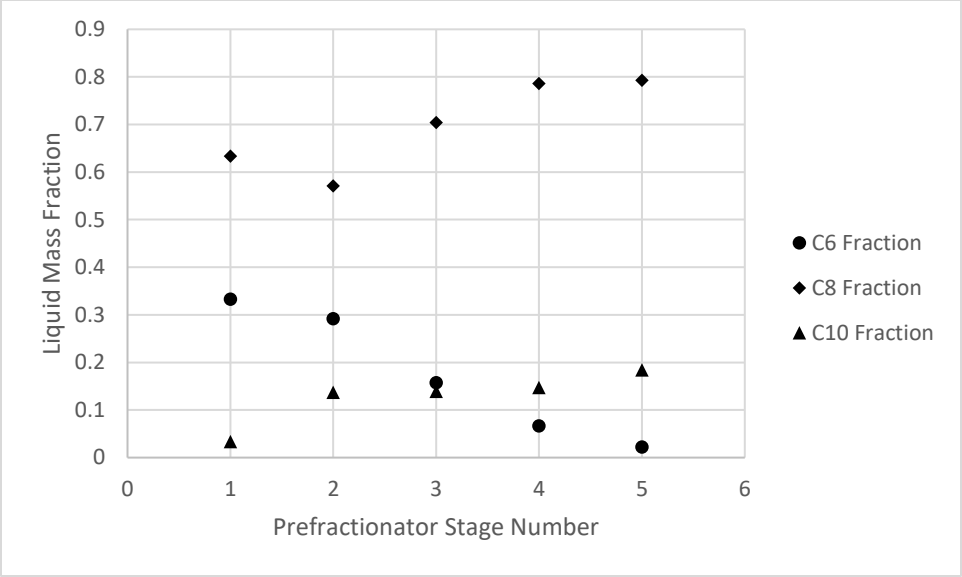

Figure 13. Liquid phase composition profile for the prefractionator of Fieg's optimized column

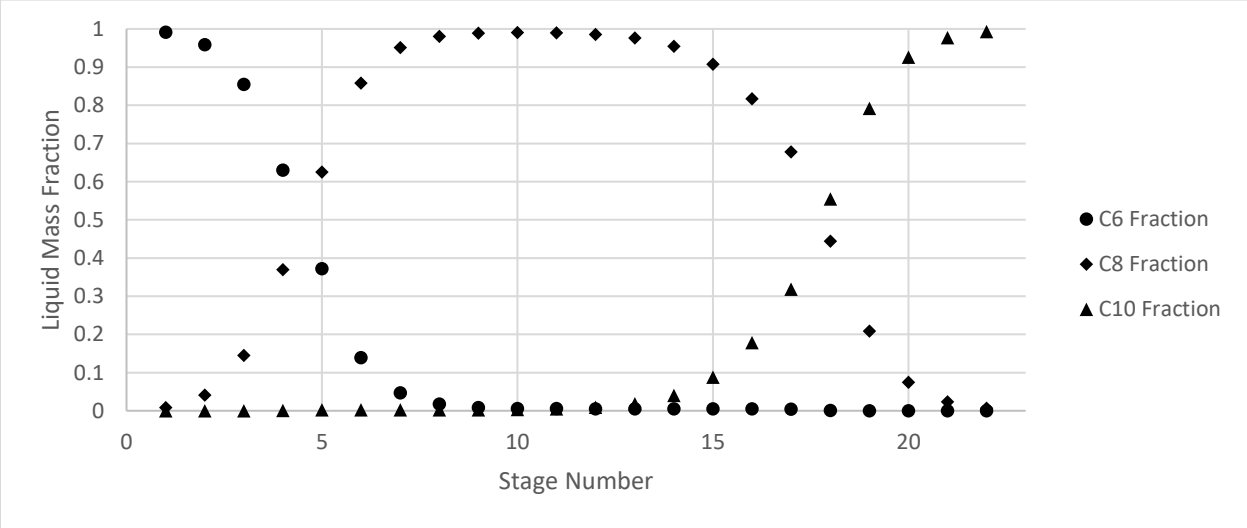

Figure 14. Liquid phase composition profile of the rectifying, stripping, and main fractionator sections for Fieg's optimized column

Compared to Dwivedi's column and Mutalib's column, the Fieg column is much smaller, with only 25 equilibrium stages. The reasoning can be explained by the K-values and the relative volatilities for the components at the feed temperature, as shown in Table 4. Compared to the other two separations, the mixture fed to the Fieg column is much easier to separate. The ease of

separation explains why the number of equilibrium stages in the column is small relative to the other two columns. The prefractionator of Fieg's column, similar to Mutalib's prefractionator, separates the light key and heavy key. The middle key is split between the top and bottom of the prefractionator. The rectifying section removes 1-octanol from the 1-hexanol to obtain a distillate with a high mass fraction for the light key. Again, the side draw is placed between the two stages where the 1-octanol mass fraction is highest. Lastly, the stripping section ensures that 1-octanol does leave the column through the bottoms, resulting in 99.3 wt% 1-decanol out the bottom of the column.

Figure 15 shows the temperature profile for Fieg's optimized column. The profile has well-defined sigmoidal sections, indicating the areas where the separation is greatest. The side draw is located at the tail ends of the two sigmoidal-shaped sections.

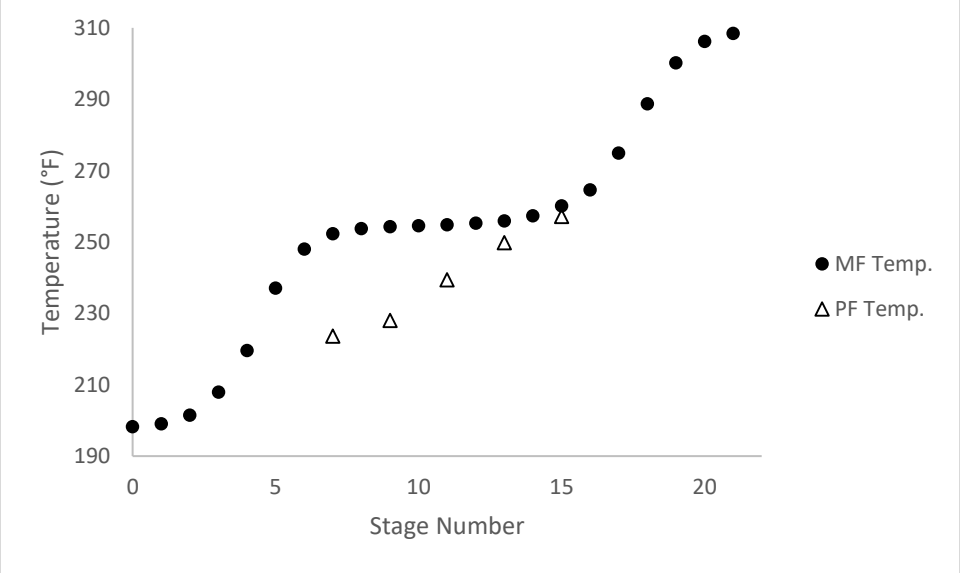

Figure 15. Temperature profile for Fieg's optimized column

HEAT TRANSFER & SCALE-UP

For each optimized case, heat transfer was implemented in two additional simulations, one with only heat loss to the atmosphere and one with both heat loss to the atmosphere and heat transfer across the dividing wall. The temperature profile in the base optimized case is used to predict the temperature profile in the heat transfer simulations. The results of each individual heat transfer implementation and scale-up will now be discussed.

Heat Transfer Implementation and Scale-Up of Dwivedi's Optimized Column

From the scale-up and heat transfer implementation, eight more simulations for the Dwivedi column were conducted. The base case Dwivedi column has a diameter of 0.229'. The effect of the scale-up/heat transfer implementation on pertinent design variables is shown in Table 12. For the Dwivedi pilot scale columns, the feed was kept constant rather than the rectifying section liquid loading (as is stated in the scale-up process flow diagram), in order to compare the effect of the heat transfer incorporation.

Table 12. Simulation results of heat transfer implementation and scale-up for Dwivedi's optimized columns

Design Variable		Units	No Heat			Heat Loss Atmosphere			Heat Loss & Heat Transfer		
Column Diameter		ft	0.229	2	10	0.229	2	10	0.229	2	10
Uatm		W/m2K	-	-	-	14	14	14	14	14	14
Uwall		W/m2K	-	-	-	-	-	-	300	300	300
Feed Flow		kg/hr	2.225	169	4228	2.225	169	4228	2.225	169	4228
Reflux Ratio		unitless	19.76	19.76	19.76	19.76	19.76	19.76	19.76	19.76	19.76
Product Purity	Ovhd, LK	mole fraction	0.9991	0.9991	0.9991	0.9992	0.9991	0.9991	0.9993	0.9991	0.9991
	Sidedraw 1, MK1		0.9912	0.9913	0.9913	0.949	0.9926	0.992	0.8403	0.9775	0.9928
	Sidedraw 2, MK2		0.9931	0.9931	0.9931	0.958	0.9944	0.9937	0.8727	0.9816	0.9945
	Bottom, HK		0.9994	0.9994	0.9994	0.9997	0.9994	0.9994	0.9988	0.9995	0.9994
Reboiler Duty		kbtu/hr	5.94	451	11285	13.575	517.5	11615	13.538	517.3	11615
Liquid Loading	Rectifying	gpm/ft2	0.721	0.723	0.723	0.731	0.724	0.723	0.731	0.724	0.723
	PF		0.653	0.655	0.655	0.891	0.677	0.659	0.981	0.697	0.660
	Upper MF		0.956	0.958	0.959	1.185	1.146	0.964	1.244	0.990	0.963
	Mid MF		1.066	1.068	1.069	1.581	1.124	1.079	1.745	1.141	1.082
	Lower MF		1.235	1.237	1.239	2.294	1.361	1.263	2.482	1.385	1.269
	Stripping		1.605	1.609	1.611	2.979	1.761	1.641	2.889	1.770	1.641
F-Factor	Rectifying	ft/s (lbm/ft3)^ 0.5	0.290	0.290	0.291	0.315	0.293	0.291	0.315	0.293	0.291
	PF		0.336	0.336	0.337	0.555	0.368	0.342	0.557	0.375	0.347
	Upper MF		0.337	0.337	0.338	0.432	0.348	0.340	0.417	0.347	0.339
	Mid MF		0.371	0.372	0.372	0.531	0.385	0.375	0.535	0.371	0.371
	Lower MF		0.389	0.389	0.390	0.706	0.426	0.397	0.718	0.428	0.397
	Stripping		0.431	0.431	0.432	0.905	0.485	0.442	0.888	0.486	0.442

From the scale-up process, the absolute flows throughout the column increased due to an increase in the feed flow. Focusing on the no heat loss columns, outside of the increased flows throughout the column and the increased reboiler duty to compensate, the product purities, liquid loadings, and F-factors remained the same, as is expected. For the three pilot size columns (0.229 feet diameter), the incorporation of heat transfer decreased the side draw product purities and increased the liquid loadings and F-factors throughout all of the column sections, in some cases to twice the original values of the no heat loss case. The reasoning behind this will be discussed later, during the temperature profile discussion.

As the column diameter increased, the product purities, liquid loadings, and F-factors all approached the base case values, for both the atmospheric heat loss cases and the atmospheric heat loss cases plus heat transfer across the wall cases. Thus, even though the magnitude of the heat loss/transfer increased due to the increased heat transfer area, the column parameters became less affected as the diameter of the column was increased.

The temperature profile for the optimized Dwivedi column (without heat loss or heat transfer) is shown in Figure 16. As is expected, the temperature rises from the bottom of the column to the top and the MF and PF have nearly the same temperature profile.

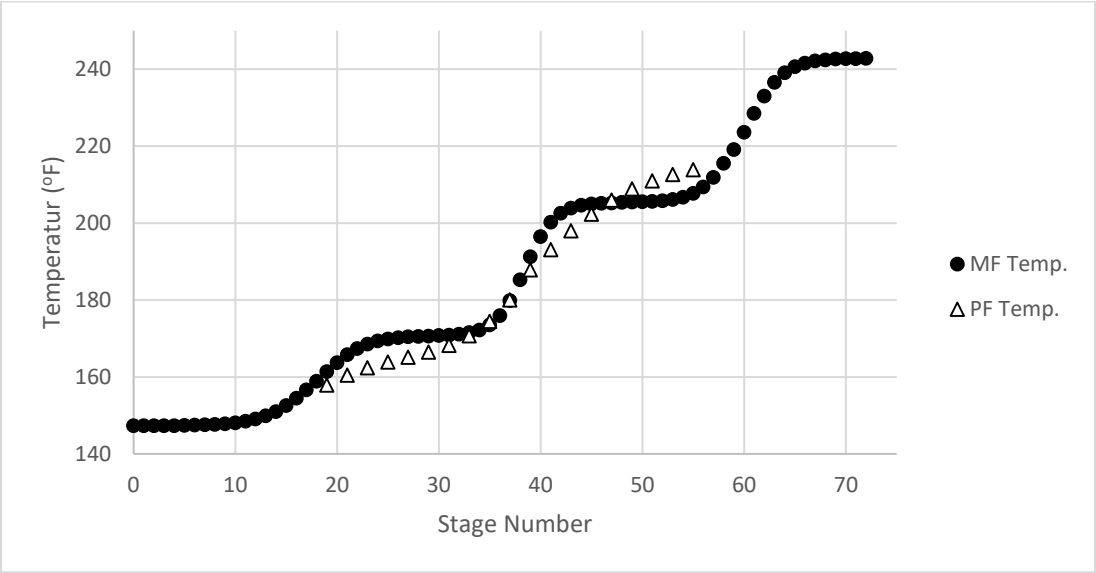

Figure 16. Temperature profile for Dwivedi's optimized column

Figure 17 shows the difference between the optimized case stage temperature and the stage temperature with heat loss to the atmosphere (calculated from the optimized case temperature profile) for the pilot scale column with a 0.229 feet diameter. At the top and bottom of the column (rectifying and stripping sections), the temperatures vary little between the two cases. However, throughout the prefractionator and the MMF, the temperature differences vary up to -30^{o}F and 20^{o}F, respectively. From the trend shown in the graph, higher values of heat lost are required in the simulation in the prefractionator. Also, the values for heat loss in the MMF should be lowered to more accurately represent that actual heat lost to the atmosphere.

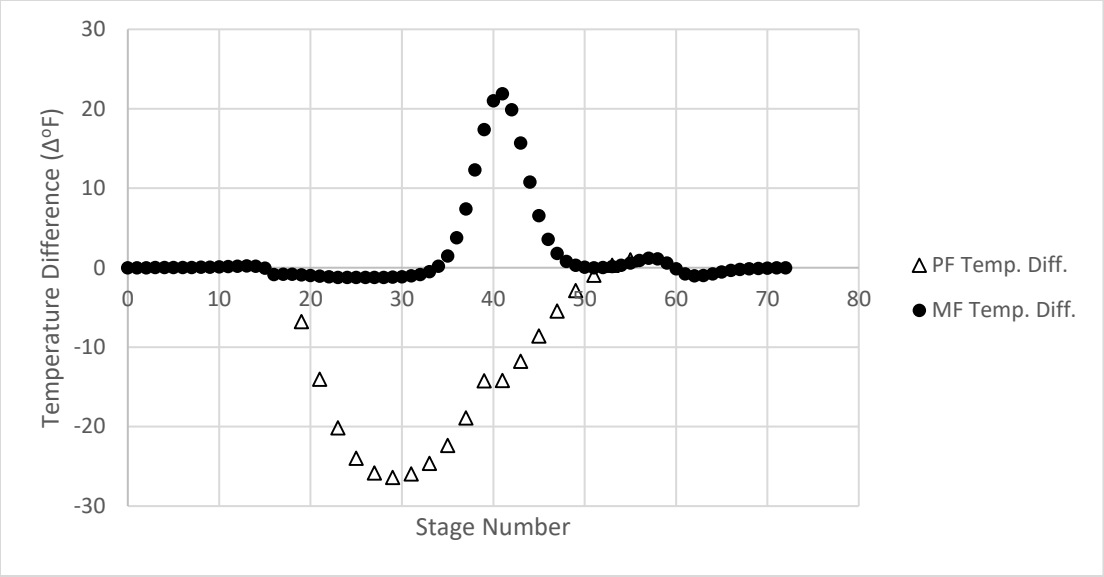

Figure 17. Stage temperature difference between the base case simulation and the heat loss to the atmosphere simulation for Dwivedi's optimized 0.229 feet diameter column

The difference between the optimized case stage temperature and the stage temperature with heat loss to the atmosphere and heat transfer across the wall is shown in Figure 18. Larger discrepancies occur in the heat transfer-included case throughout the majority of the column, with only the rectifying section matching well. Once again, the amount of heat leaving the prefractionator is underestimated. The UMF follows the same trend as the prefractionator, but at a lesser magnitude, while the MMF and the top of the stripping section have too much heat loss in the simulation. These temperature discrepancies between the cases contributes to the error in the product purities, liquid loading, and F-factors within the columns.

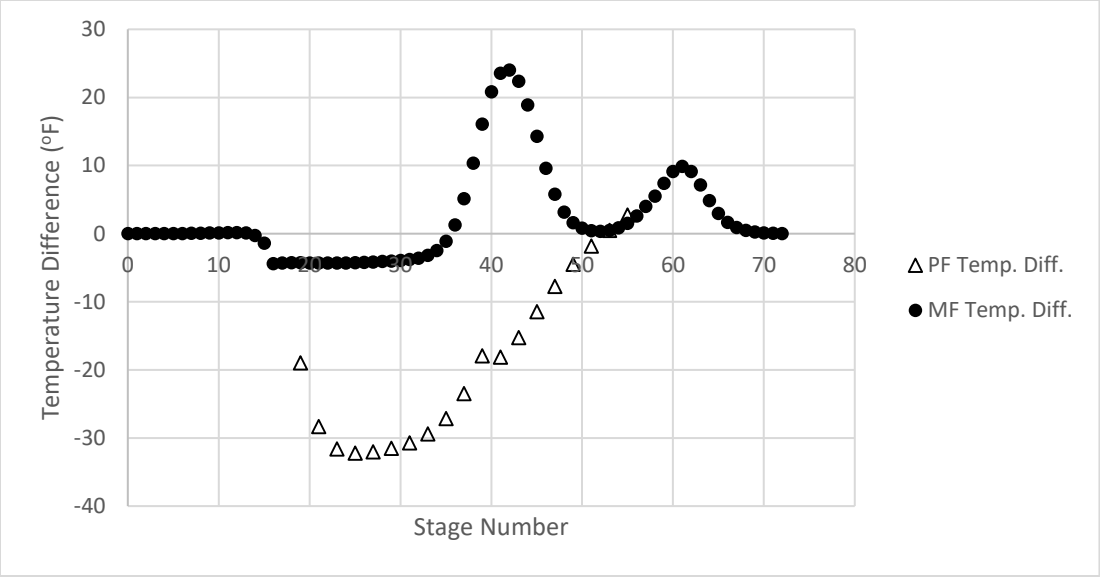

Figure 18. Stage temperature difference between the base case simulation and the heat loss to the atmosphere plus heat transfer across the wall simulation for Dwivedi's optimized 0.229 feet diameter column

The same analysis is given to the scaled-up 10 feet diameter Dwivedi column. The stage temperature differences for each stage between the no heat loss case and the heat loss to the atmosphere case are shown in Figure 19.

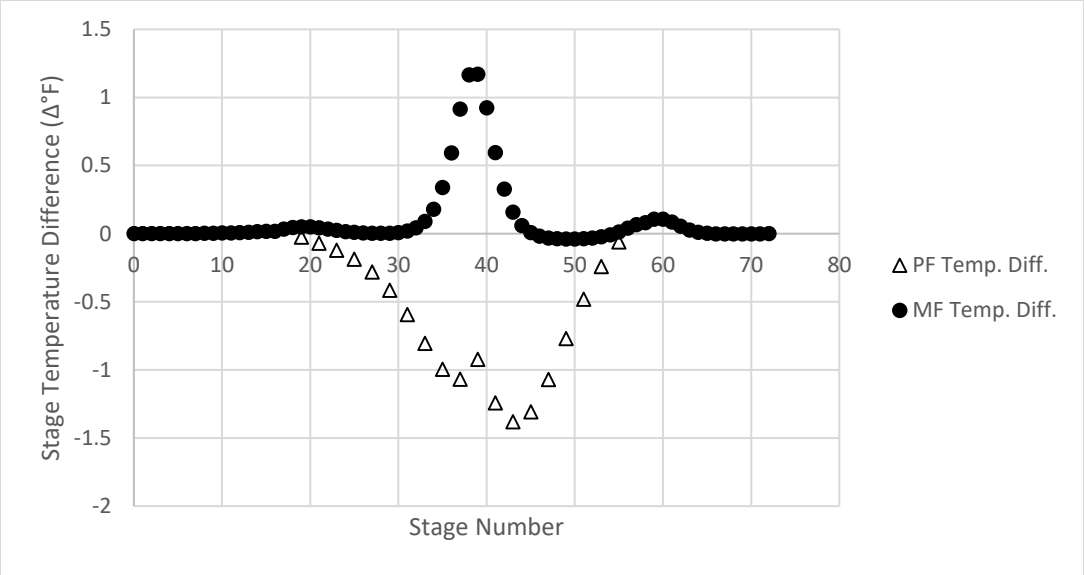

Figure 19. Stage temperature difference between the base case simulation and the heat loss to the atmosphere simulation for Dwivedi's optimized 10 feet diameter column

A similar trend is experienced in the 10’ diameter column, with a majority of the prefractionator and the middle section of the main fractionator showing a temperature difference between the two cases. However, the temperature differences have a significantly smaller magnitude than those of the pilot scale column, meaning that the temperature approximation improved with an increased diameter. The same graph is generated for the difference between the no heat loss case and the atmospheric heat loss plus heat transfer across the wall case, shown in Figure 20.

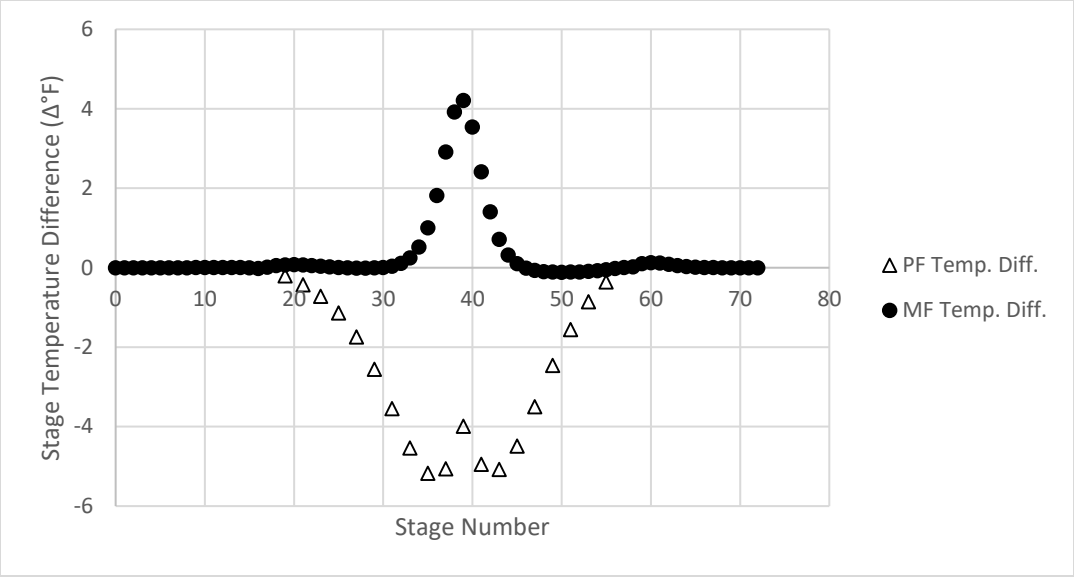

Figure 20. Stage Temperature difference between the base case simulation and the heat loss to the atmosphere plus heat transfer across the wall simulation for Dwivedi's optimized 10 feet diameter column

Again, the prefractionator and MMF trend occurs, but the magnitudes are slightly higher than in Figure 19. However, compared to Figure 18, the differences are, again, significantly smaller in magnitude than the differences for the pilot column size cases.

In terms of operating efficiency, the Dwivedi column lies in the middle of the desirable operating range, the limits of which are discussed under the Mutalib column heat loss/scale-up section. The vapor velocity through the column lies within [1.597,7.282] and the liquid loading within [0.321,0.715], as shown in Table 13. The liquid loading and vapor velocity pairs indicate that the stage pressure drop throughout the column ranges from 0.1 mbar/m in the prefractionator up to 0.5 mbar/m in the stripping sections of the two pilot columns with heat loss, in general low pressure drops throughout the columns. The pressure drop throughout the column was set by each column section (40 mm H_2O (3.92 mbar) for the rectifying and stripping sections, 20 mm H_2O (1.96 mbar) for each main fractionator section, and 60 mm H_2O (5.88 mbar) for the prefractionator) based on the pressure drop data in the literature. With an HETP of 16 cm/stage[10], the approximate

pressure drop per stage based off of the hydraulic data and Figure 21 is 0.016 mbar/stage (0.16 mm H_2O/stage). The pressure drop inputted into the simulation is nearly a magnitude larger than this, but Figure 21 is very general and the structured packing used in Dwivedi's column could deviate largely from the generic case.

Table 13. Liquid loading and vapor velocity for Dwivedi's optimized columns

			Simulations								
Design Variable		**Units**	**No Heat**			**Heat Loss Atmosphere**			**Heat Loss & Heat Transfer**		
Column Diameter		ft	0.229	2	10	0.229	2	10	0.229	2	10
Liquid Loading	**Rectifying**	m3/m2*h	1.764	1.767	1.768	1.786	1.769	1.768	1.787	1.770	1.769
	PF		1.597	1.600	1.602	2.179	1.656	1.612	2.399	1.705	1.615
	Upper MF		2.336	2.341	2.345	2.896	2.803	2.356	3.042	2.421	2.355
	Mid MF		2.606	2.610	2.613	3.865	2.747	2.639	4.266	2.789	2.644
	Lower MF		3.020	3.025	3.028	5.608	3.327	3.088	6.068	3.385	3.102
	Stripping		3.924	3.935	3.939	7.282	4.306	4.011	7.064	4.327	4.012
Vapor Velocity	**Rectifying**	m/s	0.325	0.325	0.326	0.353	0.329	0.326	0.353	0.329	0.326
	PF		0.321	0.322	0.322	0.495	0.342	0.326	0.491	0.343	0.326
	Upper MF		0.323	0.324	0.324	0.414	0.334	0.326	0.396	0.332	0.326
	Mid MF		0.327	0.328	0.328	0.499	0.347	0.332	0.503	0.345	0.331
	Lower MF		0.331	0.332	0.332	0.602	0.363	0.338	0.612	0.364	0.338
	Stripping		0.341	0.341	0.341	0.715	0.384	0.350	0.708	0.384	0.350

Heat Transfer Implementation and Scale-Up of Mutalib's Optimized Column

Table 14 shows the process of scale-up and heat transfer incorporation, and its effects on the column operation, for the Mutalib column. The pilot scale Mutalib column has a diameter of 1 foot. The scale-up procedure for the Mutalib columns follows the flow diagram of Figure 7.

Table 14. Simulation results of heat transfer implementation and scale-up for Mutalib's optimized column

Design Variable		Units	No Heat			Heat Loss Atmosphere			Heat Loss & Heat Transfer		
Column Diameter		ft	1	2	10	1	2	10	1	2	10
Uatm		W/m2K	-	-	-	14	14	14	14	14	14
Uwall		W/m2K	-	-	-	-	-	-	300	300	300
Feed Flow		kmol/hr	1.082	4.338	108.89	1.064	4.313	108.4452	1.064	4.297	108.4452
Reflux Ratio		unitless	3.11	3.12	3.12	3.12	3.12	3.12	3.12	3.12	3.12
Product Purity	Ovhd, LK	mole fraction	0.9923	0.9948	0.9948	0.9969	0.9963	0.9954	0.9938	0.995	0.9952
	Sidedraw, MK		0.9913	0.9894	0.9894	0.994	0.9928	0.9906	0.988	0.9904	0.9903
	Bottom, HK		0.9989	0.9988	0.9988	0.9998	0.9996	0.9991	0.9992	0.9996	0.9992
Reboiler Duty		kbtu/hr	22.5	210	5270	88.8	283.4	5625	88.45	282	5625
Liquid Loading	Rectifying	gpm/ft2	0.273	0.272	0.273	0.272	0.273	0.273	0.272	0.272	0.273
	PF		0.164	0.163	0.164	0.240	0.201	0.171	0.242	0.203	0.171
	Upper MF		0.713	0.694	0.696	0.973	0.830	0.719	1.002	0.843	0.721
	Lower MF		0.413	0.412	0.413	0.819	0.618	0.454	0.971	0.693	0.470
	Stripping		0.876	0.875	0.878	1.321	1.099	0.922	1.241	1.097	0.926
F-Factor	Rectifying	ft/s (lbm/ft3)^ 0.5	0.142	0.141	0.142	0.155	0.149	0.143	0.156	0.149	0.143
	PF		0.151	0.151	0.151	0.215	0.183	0.157	0.211	0.180	0.157
	Upper MF		0.170	0.168	0.169	0.226	0.197	0.174	0.206	0.188	0.172
	Lower MF		0.173	0.173	0.174	0.256	0.215	0.182	0.264	0.220	0.183
	Stripping		0.191	0.191	0.192	0.312	0.253	0.204	0.306	0.251	0.204

Many of the trends discussed in the Dwivedi scale-up/heat transfer section are evident in the Mutalib columns as well. One interesting difference is the scale-up of the no heat loss case. The side draw product decreased slightly below the purity specification desired, even though the reflux ratio and liquid loading in the rectifying section values match the values of the base case. Upon heat loss and/or heat transfer incorporation, the side draw purity increased back to the correct purity specification. Thus, even though most simulations lack the effects of heat transfer, it is important that the final simulation takes into account heat transfer throughout the column.

An important area of operation of a standard distillation column is the hydraulics of the liquid and vapor flows within the column. All of the columns in this study are structured packing columns, so the hydraulics of the column are critical for increasing the mass transfer efficiency between the two phases, maximizing the number of theoretical stages per height of the column (HETP), and minimizing the pressure drop per stage.[17] Figure 21 shows the operating, dewetting and flooding operation zones for a standard packed distillation column, as discussed by the KLM Technology Group.[17]

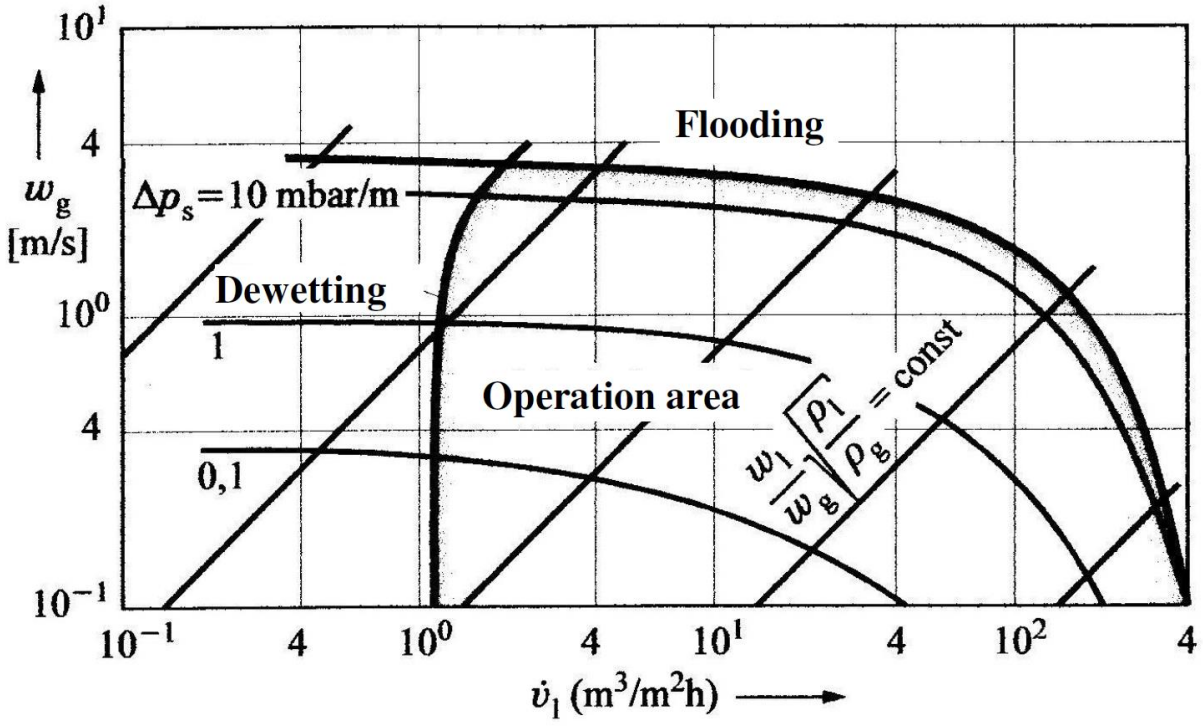

Figure 21. Standard column operation zones for packed distillation columns, as defined by KLM Technology Group[17]

KLM Technology Group bases their zoning off of the vapor velocity (in m/s) through the packing and the liquid loading (in m^3/m^2h). Table 15 shows the vapor velocity and liquid loading (in m^3/m^2h) for the nine heat transfer/scale-up simulations for the Mutalib column.

Table 15. Liquid loading and vapor velocity for Mutalib's optimized columns

			Simulations								
Design Variable		**Units**	**No Heat**			**Heat Loss Atmosphere**			**Heat Loss & Heat Transfer**		
Column Diameter		ft	1	2	10	1	2	10	1	2	10
Liquid Loading	**Rectifying**	m3/m2h	0.667	0.666	0.669	0.665	0.668	0.667	0.665	0.666	0.668
	PF		0.401	0.398	0.400	0.586	0.493	0.417	0.593	0.496	0.419
	Upper MF		1.743	1.696	1.702	2.378	2.028	1.758	2.450	2.060	1.763
	Lower MF		1.011	1.007	1.011	2.002	1.511	1.110	2.375	1.695	1.150
	Stripping		2.141	2.140	2.147	3.231	2.688	2.254	3.033	2.682	2.265
Vapor Velocity	**Rectifying**	m/s	0.156	0.157	0.158	0.174	0.166	0.159	0.172	0.165	0.159
	PF		0.147	0.147	0.148	0.202	0.176	0.153	0.197	0.172	0.153
	Upper MF		0.148	0.148	0.149	0.198	0.174	0.154	0.183	0.166	0.152
	Lower MF		0.147	0.147	0.148	0.218	0.183	0.154	0.224	0.186	0.155
	Stripping		0.153	0.154	0.154	0.250	0.202	0.164	0.246	0.202	0.164

The domain (liquid loading) of values falls within [0.398, 3.231] and the range (vapor velocity) is [0.147, 0.250]. Looking at Figure 21 again, the prefractionator and rectifying sections lie within the dewetting region of operation, an area characterized by the formation of droplets from the thin film, allowing vapor to flow by without contacting the liquid phase and inhibiting mass transfer. The LMF, depending on the heat transfer implementation and the column diameter, teeters between the operating and dewetting zones. To improve the operation of these three sections, the cross-sectional flow area should be decreased or the reflux should be increased, thus increasing the amount of flow through the sections. The UMF and stripping sections are well within the operation zone, and correspond to very low stage pressure drops, around approximately 0.05 mbar/m. The remaining sections (the dewetting sections) have low pressure drops on the magnitude of 0.005 mbar/m, most likely due to the lack of full film development on the packing.

In the Mutalib simulation, the pressure drop was assumed to be 0.01 bar/section for the rectifying, stripping, and prefractionator sections and 0.005 bar/section for the UMF and LMF sections, as Mutalib did not give pressure drops for the column sections. The GEMPAK 4A packing used in the Mutalib column has an HETP of approximately 0.3324 m/stage. For the dewetting sections, this corresponds to 1.66×10^{-3} mbar/stage and 1.66×10^{-2} mbar/stage for the operational zone sections (UMF and stripping). The approximations for the pressure drops in the column were, again, different by an order of magnitude between the simulation input and the predicted pressure drop.

Heat Transfer Implementation and Scale-Up of Fieg's Optimized Column

The results of scale-up and heat transfer implementation on the column operation for the Fieg column is shown in Table 16. The pilot scale diameter for Fieg's column is 0.223 feet. Similar to Dwivedi, the pilot scale columns had matching feed flows rather than matching liquid loading in the rectifying section to observe the effects on design variables.

Table 16. Simulation results of heat transfer implementation and scale-up for Fieg's optimized column

Design Variable		Units	No Heat			Heat Loss Atmosphere			Heat Loss & Heat Transfer		
Column Diameter		ft	0.223	2	10	0.223	2	10	0.223	2	10
Uatm		W/m2K	-	-	-	14	14	14	14	14	14
Uwall		W/m2K	-	-	-	-	-	-	300	300	300
Feed Flow		kg/hr	2.5	201	5035	2.5	200	5035	2.5	201	5035
Reflux Ratio		unitless	2.32	2.32	2.32	2.32	2.32	2.32	2.32	2.32	2.32
Product Purity	Ovhd, LK	mass fraction	0.9936	0.9936	0.9936	0.996	0.9946	0.9939	0.7863	0.9953	0.9944
	Sidedraw, MK		0.9903	0.9902	0.9902	0.9932	0.9915	0.9905	0.7548	0.9906	0.991
	Bottom, HK		0.9936	0.9935	0.9935	0.9945	0.994	0.9937	0.9503	0.9906	0.9932
Reboiler Duty		kbtu/hr	2.49	200	5010	6.62	233.6	5185	6.72	236	5190
Liquid Loading	Rectifying	gpm/ft2	0.485	0.485	0.486	0.527	0.487	0.487	0.554	0.485	0.487
	PF		0.279	0.277	0.277	0.497	0.299	0.282	0.251	0.274	0.277
	Upper MF		0.807	0.799	0.801	1.120	0.828	0.807	1.257	0.819	0.805
	Lower MF		0.561	0.560	0.561	1.300	0.639	0.578	1.929	0.726	0.595
	Stripping		0.949	0.949	0.951	1.973	1.059	0.974	2.003	1.058	0.975
F-Factor	Rectifying	ft/s (lbm/ft3)^ 0.5	0.516	0.516	0.517	0.584	0.521	0.518	0.601	0.519	0.518
	PF		0.580	0.558	0.559	1.069	0.630	0.591	1.210	0.657	0.597
	Upper MF		0.623	0.615	0.616	0.874	0.647	0.629	0.405	0.598	0.620
	Lower MF		0.620	0.619	0.621	1.140	0.675	0.633	1.093	0.673	0.633
	Stripping		0.632	0.640	0.633	1.488	0.725	0.653	1.466	0.717	0.652

In terms of trends, the expected trends observed in the Mutalib and Dwivedi columns are found in the Fieg optimized cases. However, between the heat loss to the atmosphere only pilot scale case and the heat loss and heat transfer pilot scale case, there are large differences in the purities, but barely only slight differences in the liquid loading and F-factor values throughout the columns. The Fieg case, especially at smaller diameters, emphasizes the importance of modeling the heat transfer across the dividing wall. With only heat loss to the atmosphere modeled at the pilot scale level, the product purities easily meet the specifications as desired. However, upon incorporation of heat transfer across the wall, all three purities, especially the light key and middle key, drop significantly to the point where the design is largely flawed. Though these differences

are mitigated with an increasing diameter, the best model includes the operation of the column, the mass transfer phenomena occurring within, the heat transfer across the wall, and the hydraulics experienced within the column.

Table 17. Liquid loading and vapor velocity for Fieg's optimized columns

			Simulations								
Design Variable		**Units**	**No Heat**			**Heat Loss Atmosphere**			**Heat Loss & Heat Transfer**		
Column Diameter		ft	0.223	2	10	0.223	2	10	0.223	2	10
Liquid Loading	**Rectifying**	m3/m2*h	1.186	1.185	1.187	1.288	1.190	1.190	1.354	1.186	1.190
	PF		0.682	0.677	0.678	1.216	0.730	0.690	0.612	0.669	0.677
	Upper MF		1.973	1.953	1.957	2.738	2.025	1.974	3.074	2.003	1.968
	Lower MF		1.372	1.368	1.371	3.179	1.563	1.413	4.716	1.775	1.456
	Stripping		2.320	2.319	2.324	4.823	2.588	2.381	4.896	2.587	2.383
Vapor Velocity	**Rectifying**	m/s	1.196	1.196	1.199	1.358	1.209	1.203	1.335	1.205	1.203
	PF		1.253	1.237	1.239	2.268	1.357	1.276	2.552	1.401	1.286
	Upper MF		1.326	1.316	1.319	1.862	1.377	1.338	0.908	1.274	1.319
	Lower MF		1.307	1.305	1.308	2.397	1.421	1.333	2.313	1.417	1.333
	Stripping		1.257	1.257	1.259	2.956	1.441	1.298	3.007	1.434	1.298

Table 17 shows the liquid loading and vapor velocity throughout the column, as pertaining to the corresponding units in Figure 21. The prefractionator section is the only column section with dewetting whereas the remaining column sections span vertically across the left region of the operating zone. The pilot scale columns with heat loss and/or heat transfer, show the largest variations ($\pm$ 2 m/s) in vapor velocity throughout the column whereas the other simulations show variations of $\pm$ 0.1 m/s. For the larger-than-pilot diameter columns, the pressure drops experienced throughout the column are relatively high compared to the Dwivedi and Mutalib columns, with values of approximately 2 mbar/m. The published HETP for the packing in the Fieg column is 0.196 m/stage, yielding a pressure drop of 0.396 mbar/stage. The pressure drop in the simulation varies by section: the prefractionator and rectifying sections have 0.6 mbar/stage, the UMF and LMF have 0.3 mbar/stage, and the stripping section has 0.45 mbar/stage, all based off the pressure drops given in the literature. The predicted stage pressure drop, which is 0.396 mbar/stage, was close to the simulation input pressure drop. The largest average difference in the prefractionator

and the rectify sections varied by only 51.5% at most. In terms of the pressure profile that would be experienced within the column, the Fieg simulation matched the prediction the best compared to Mutalib's and Dwivedi's columns.

Sources of Error

Because Aspen does not have a rigorous, multivariable model for the DWC, there is potential for sources of error in the simulations of the three columns studied. Firstly, there is not an established rule for the number of stages that must be present in the prefractionator and main fractionator. In this study, the number of stages between the two sections was allowed to vary, with some simulations having twice as many stages in the main fractionator as there are in the prefractionator. This can pose a problem as the heat transfer across the dividing wall relies on contact between the liquid and vapor phase on the prefractionator side with the wall and the liquid and vapor phase on the main fractionator side with the wall. To approximate the heat transfer in this study, stages on the side with fewer stages were split and the temperature between stages was predicted linearly based on the temperatures given by the simulation. These split stage temperatures were then paired with stage temperatures on the other side of the wall in order to approximate the heat transfer. For packed columns, one way to alleviate this problem is to utilize different packing on each side of the dividing wall. The packing can be chosen based on the HETP. The side of the wall that requires more stages should have packing with a lower HETP in order to allow for more theoretical stages within the same height of the column.

Another form of error comes from the pressure estimations used in the simulations and the method used to predict the pressure drops in the column based on the data given by the KLM Technology group. Figure 21 is based off of cylindrical geometry packing, which is not a problem in the rectifying and stripping sections of DWCs. However, in the prefractionator and main fractionator, the packing is semi-cylindrical in shape, in order to fit between the dividing wall and the shell of the column. In a DWC, as a condition of steady state, the pressure drop on each side of the wall must be equal. If the packing on each side of the wall doesn't have an equivalent

pressure drop, then more vapor will flow to the side of the wall with the lower pressure drop until an equilibrium state is reached. Special consideration should be given to this if the number of stages or the packing type is different on each side of the wall.

Lastly, the way HEEDS operates in this study compared to other optimization functions is critical in the evaluation of the optimization. In all of the simulations, HEEDS serves as a command script that yields the Aspen input file from which Aspen Plus runs a simulation. All of the material and energy balance calculations are performed within the Aspen engine. Thus, without further interconnection between HEEDS and Aspen Plus, the amount of control over the design equations that govern the DWC model is limited to the current implementation in Aspen Plus. In other words, HEEDS can be a more effective optimization tool if there is an increased interconnection with Aspen Plus in the form of what equations are solved when running a simulation and which variables are prioritized when optimizing the base case. For example, in this paper, to model heat transfer across the wall, the temperature profile was predicted from the base case simulation and, using Equation 1, the heat transfer for each stage was directly inputted within the simulation, rather than being based off of the actual temperature of the stage. Aspen's lack of a model for heat transfer between two column stages reduces the validity of the model. If HEEDS were more interconnected to the code that Aspen Plus executes when solving the stage equilibrium problem, HEEDS could input specific values for the temperature at each iteration, calculate the heat transfer, and better model the heat transfer phenomena that occurs at the dividing wall.

Conclusion

In this work, three pilot scale, DWCs found in literature are studied. Using a new systematic method, Aspen Plus, a rigorous process modeler, is connected to HEEDS, an interdisciplinary optimization program, in order to manipulate the design variables that govern the model used to simulate the DWC and to run thousands of simulations to optimize the base case pilot scale DWCS as well as observe the trends noted. The new HEEDS-Aspen Plus method is less rigorous in setup compared to other optimization methods mentioned[7-9], and uses the new SHERPA optimization method designed by Red Cedar Technologies, the developers of the HEEDS optimization software. The SHERPA method is highly efficient, with an optimized solution typically being found using the aforementioned long-range method (large search field) within a thousand simulations. HEEDS takes advantage of the previously setup Aspen Plus engine while offering ease in terms of user interface connections and ability to tune optimization parameters to the goals of the optimization.

Following is a discussion of the changes between the optimized case and the base case simulations, the function of each section modeled in Aspen Plus and how the components being separated govern the component compositions and the pertinent design variables throughout each section of the DWC. The Dwivedi and Mutalib columns saw increases in the capital cost based design variables (number of stages per section, feed location, side draw location, etc.) in order to meet the required product specification and decreases in operational cost based design variables (reboiler duty, reflux ratio, etc.) whereas Fieg's column saw reductions in both compared to the base case.

Next, heat transfer across the dividing wall and heat loss to the atmosphere were calculated and implemented into each case and scale-ups from pilot scale to 2 ft and 10 ft diameter columns

occurred to study any changes in design variables and observe the effects of heat transfer. In general, heat transfer had a larger effect on smaller diameter columns, mainly the pilot scale DWCs where in some cases products were thrown out of specification by heat transfer modeling. As the diameter increased, even though heat transfer and heat loss increased with the increasing heat transfer area, the effects on the column purities and hydraulics decreased to the point in the 10 ft diameter columns there was little to no change from the base case. The column hydraulics of each optimized case is studied and the pressure drops throughout the column are discussed.

Finally, errors in the model and HEEDS-Aspen Plus method are evaluated and the suggestion of using HEEDS to further manipulate how Aspen Plus sets up and executes solving the design equations that govern the equilibria, mass transfer, and heat transfer phenomena that are experienced in a DWC is given to further the validity and accuracy of the DWC model in Aspen Plus, with a focus on the effects of DWC specific variables, including the vapor and liquid splits, the placement of the dividing wall, and the side draw location. HEEDS in conjunction with Aspen Plus has proven to be a powerful tool in optimizing the three studied DWCs and more effort put into linking the two programs can yield simulations that are more accurate than available in Aspen Plus on its own.

Appendix A – Symbols List

A	Area
B	Bottoms
D	Distillate
DWC	Dividing Wall Distilation Column
ΔT	Change/Difference in temperature
HEEDS	Multidisciplinary Optimization Software linked with Aspen Plus
HETP	Height Equivalent to the Theoretical Plate
HK	Heavy Key
L_{Rect}	Liquid Loading in the Rectifying Section
L_{Spl}	Liquid Split
LK	Light Key
LMF	Lower Main Fractionator
MF	Main Fractionator
MK	Middle Key
MMF	Middle Main Fractionator
N	Number of Stages
PF	Prefractionator
Q	Heat Duty
R_R	Reflux Ratio
S	Side Draw
SHERPA	Simultaneous Hybrid Exploration that is Robust, Progressive, and Adaptive
U	Overall Heat Transfer Coefficeint
UMF	Upper Main Fractionator
V_{Spl}	Vapor Split

References

[1]Wright, R. O.; Elizabeth, N. J. Fractionation Apparatus. U.S. Patent 2,471,134, May 24, 1949.

[2]Triantafyllou, C.; Smith, R. The Design and Optimization of Fully Thermally Coupled Distillation-Columns. *Chem. Eng. Res. Des.* 1992, *70*, 118.

[3]Hernandez, S.; Jimenez, A. Design of Energy-Efficient Petyluk Systems. *Comput. Chem. Eng.* 1999, *23*, 1005.

[4]Wolff, E. A.; Skogestad, S. Operations of Integrated 3-product Petyluk Distillation- Columns. *Ind. Eng. Chem. Res. Des.* 1988, 66, 229.

[5]Glinos, K.; Malone, M.F. Optimality Regions for Complex Column Alternatives in Distillation Systems. *Chem. Eng. Res. Des.* 1988, *66*, 229.

[6]Schultz, M.A.; Stewart, D. G.; Harris, J.M.; Rosenblum, S. P.; Shakur, M. S.; O'Brien, D. E. Reduce Costs with Dividing-Wall Columns. *Chem. Eng. Prog.* 2002, *98*, 64.

[7]Pattison, R. C.; Gupta, A. M.; Baldea, M. Equation-Oriented Optimization of Process Flowsheets with Dividing Wall-Columns. *AIChE Journal 2015, 62* (3), 704-716. Richard C. Pattison, Akash M. Gupta, and Michael Baldea.

[8]Gómez-Castro, F. I.; Segovia-Hernández, J. G.; Hernández, S.; Gutiérrez-Antonio, C.; Briones-Ramírez, A. Dividing Wall Distillation Columns: Optimization and Control Properties. *Chemical Engineering & Technology* 2008, *31* (9), 1246-1260.

[9]Ge, X.; Yuan, X.; Ao, C.; Yu, K.-K. Simulation Based Approach to Optimal Design of Dividing Wall Column using Random Search Method. *Computers & Chemical Engineering* 2014, *68*, 38–46.

[10]Dwivedi, D. Control and operation of dividing-wall columns with vapor split manipulation. dissertation, Norwegian University of Science and Technology: Trondheim, 2013.

[11]Mutalib, M. I. A. Operation and Control of the Dividing Wall column. dissertation, Department of Process Integration: Manchester, 1995.

[12]Niggemann, G.; Hiller, C.; Fieg, G. *Industrial & Engineering Chemistry Research*2010, *49* (14), 6566–6577.

[13]HEEDS. http://www.redcedartech.com/products/heeds_mdo (accessed May 10, 2017).

[14]Design and Optimize Chemical Processes with Aspen Plus®. http://origin-www.aspentech.com/products/aspen-plus.aspx (accessed May 10, 2017).

[15]Noweck, K.; Grafahrend, W. Fatty Alcohols. In *Ulmann's Encyclopedia of Industrial Chemistry*: Wiley -VCH: Weinheim, 2006.

[16]SHERPA – An Efficient and Robust Optimization/Search Algorithm. 2017. 1-3.

[17]Hoon, C. Y.; Jing, A. L.; Jaya, A.; Firdaus, M. A. Engineering Design Guidelines - Distillation Column Selection and Sizing. http://www.klmtechgroup.com/ (accessed May 10, 2017).